energies

MDPI

Article

Comprehensive Performance Assessment of Dual Loop Organic Rankine Cycle (DORC) for CNG Engine: Energy, Thermoeconomic and Environment

Xu Ping, Baofeng Yao *, Hongguang Zhang *, Hongzhi Zhang, Jia Liang, Meng Yuan, Kai Niu and Yan Wang

Key Laboratory of Enhanced Heat Transfer and Energy Conservation of MOE, Beijing Key Laboratory of Heat Transfer and Energy Conversion, Faculty of Environment and Life, Beijing University of Technology, Beijing 100124, China

* Correspondence: yaobf@bjut.edu.cn (B.Y.); zhanghongguang@bjut.edu.cn (H.Z.)

Abstract: The improvement of the overall utilization rate of compressed natural gas (CNG) engine fuel is the basis of efficient energy utilization. On the foundation of heat balance theory of internal combustion engines, this study fully considers the operation characteristics of CNG engines and systematically analyzes the distribution characteristics of different waste heat under variable working conditions. The nonlinear relationship between speed and intercooler heat source becomes evident with the increasing of intake mass flow rate. In accordance with the structural characteristics, the thermodynamic model, heat transfer model and environmental model of dual-loop organic Rankine cycle (DORC) are constructed. The system potential in full working environments is systematically evaluated. Compared with the speed, airmass flow has a significant effect on comprehensive performance of loop. The maximum power, heat transfer area and power output of per unit heat transfer area (POPA) of DORC are 36.42 kW, 23.34 m^2, and 1.75 kW/m^2, respectively. According to the operating characteristics of different loops, the variation laws of loop performance under the influence of multiple parameters are analyzed. The synergistic influence laws of multiple variables on system performance are also analyzed.

Keywords: CNG engine; dual loop organic Rankine cycle; energy efficiency; thermoeconomic analysis; thermodynamic analysis; environment analysis

Citation: Ping, X.; Yao, B.; Zhang, H.; Zhang, H.; Liang, J.; Yuan, M.; Niu, K.; Wang, Y. Comprehensive Performance Assessment of Dual Loop Organic Rankine Cycle (DORC) for CNG Engine: Energy, Thermoeconomic and Environment. *Energies* **2022**, *15*, 7832. https://doi.org/10.3390/en15217832

Academic Editor: George Kosmadakis

Received: 27 September 2022
Accepted: 20 October 2022
Published: 22 October 2022

1. Introduction

Energy is vital to the development of human society. As one of the major components of energy, petroleum is widely used in internal combustion (IC) engines [1–3]. Among alternative fuels, compressed natural gas (CNG) has received extensive attention due to its low cost, abundant yield, and environmental friendliness [4]. In the process of CNG engine operation, output work produced by fuel is only a part of the total energy, while waste heat is also generated. The efficient utilization of the waste heat is beneficial to improving the overall utilization rate of fuel to save energy. As a thermal power conversion system, the organic Rankine cycle (ORC) has received great attention among waste heat utilization methods [5,6].

1.1. Working Conditions and Waste Heat Characteristics

Compared with fixed IC engines, vehicle IC engines usually operate under variable working conditions. This characteristic makes the waste heat energy of vehicle IC engines show evident fluctuation [7,8]. Under the influence of fluctuations and uncertainties, ORC usually operates under off-design conditions. This phenomenon makes ORC lack power capacity under most working conditions. Compared with the thermal efficiency in the design working condition, the thermal efficiency in the off-design working condition is remarkably reduced [9]. At low speed and idle speed, the variation of IC engine working

conditions is aggravated, which considerably enhances the hysteresis in the ORC operation process [10]. Moreover, during the operating of IC engines, the distribution of waste heat energy of the intercooler, jacket water and exhaust has remarkable differences [11], which might have a negative effect on the efficient operation of ORC. Table 1 shows the selection of IC engine working conditions. The ORC performance is affected not only by the working fluid and operating parameters, but also by the working conditions of the IC engine. The constant high-temperature heat source of IC engines has limitations with regard to the research of ORC comprehensive performance. The systematic assessment of ORC operating performance under full working conditions is fundamental to further analysis and optimization. Moreover, it is beneficial to obtaining the actual recovery potential of ORC.

Table 1. Selection of working environments of an IC engine.

Application	Year	Refs.	Working Conditions
Select the working fluid for loop organic Rankine cycle (DORC).	2020	Wang et al. [12]	The exhaust temperature and mass flow are 519 °C and 990.79 kg/h, respectively.
The operation performance of the transcritical-subcritical parallel ORC is analyzed. Based on evaluation results, the performance of the system is optimized.	2020	Zhi et al. [13]	The exhaust temperature and mass flow are 573.15 K and 1.91 kg/s, respectively.
The energy utilization efficiency and exergy efficiency of the transcritical CO_2 parallel Rankine cycle are analyzed.	2020	Zhi et al. [14]	The exhaust temperature and mass flow are 300 °C and 1.91 kg/s, respectively.
The thermodynamic and economical performance of supercritical CO_2-ORC are evaluated. Based on evaluation results, the system performance is optimized.	2020	Song et al. [15]	The exhaust temperature and mass flow are 457 °C and 1.69 kg/s, respectively.
The economy of ORC is analyzed. Furthermore, the application potential of ORC in waste heat recovery of an IC engine is analyzed.	2016	de Oliveira Neto et al. [16]	The exhaust temperature and mass flow are A and B, respectively.

1.2. Influence of Operating Parameter

By the analysis of the influence of variable working conditions, a nonlinear response characteristic emerges between the variable and index. The study by Wang et al. [17] shows that the condensing pressure decreases during the high-temperature (HT) cycle. The power of the low-temperature (LT) cycle is considerably reduced in comparison with the power of the HT cycle. Increasing the loop pressure of DORC helps to obtain higher power output. The reduction of the condensing temperature is of benefit to reducing the system recovery life [18]. Fluctuations in IC engine working condition affect the evaporating temperature in system. The increase of evaporating temperature is conducive to improvement of system performance [19]. A strong correlation exists between expander operating parameters in the loop and the thermodynamic performance of the system. Higher expander inlet pressure is conducive to the improvement of system thermal efficiency. The decrease of loop pressure can reduce exergy destruction [20].

1.3. Performance Analysis of DORC

During the operation of IC engines, the change of the waste heat source presents the characteristics of a large temperature gradient. Moreover, a strong coupling relationship exists between ORC operation parameters. Under the influence of such characteristics, the systematic analysis of ORC performance is crucial to improving the overall fuel utilization rate [21–23]. Table 2 shows the selection of ORC performance. The performance evaluation of ORC under different high-temperature heat sources has received extensive attention. The structure of ORC is complicated due to the multistage utilization of the waste heat

source. Under a complex structure, the systematic assessment of the comprehensive index is crucial for the efficient utilization of energy. A clear coupling relationship exists between the operational performance of the subloop and overall performance. A systematic analysis of the variation between the overall performance and the sub cycle is beneficial to obtaining the potential practical application of the cycle.

Table 2. Selection of index of ORC.

Index	Description	Year	Refs.
Power and efficiency	The waste heat of biomass is recovered and utilized through DORC.	2020	Fouad et al. [24]
Power and efficiency	Based on the distribution of waste heat energy in the power plant, the operational performance of two cascaded ORC is analyzed.	2020	Linnemann et al. [25]
Power and efficiency	Combine ORC, ranking cycle and absorption refrigeration cycle into a hybrid system.	2020	Liu et al. [26]
Power, exergy and thermal efficiency	The application potential of series ORC and parallel ORC in vehicle waste heat is compared.	2020	Surendran et al. [27]
Power, thermal efficiency, payback period and investment cost	The working fluid of the DORC cycle is selected. The difference of DORC operation performance under working fluids is evaluated.	2019	Mohammadkhani et al. [28]

1.4. Work and Contribution

A systematic evaluation of waste heat source characteristics of IC engines with variable working conditions is crucial for the comprehensive performance of DORC analysis. According to the heat balance theory of IC engines, this study fully considers the operating characteristics and systematically analyzes waste heat distribution of the different operating environment. On the basis of the structural feature in DORC, the thermodynamic sub-model, heat transfer model, thermoeconomic model, and environmental model are constructed. The HT and LT cycle models are then coupled and correlated to construct the DORC thermodynamic sub-model, heat transfer sub-model, thermoeconomic sub-model, and environmental sub-model. A clear coupling relationship exists between the operational performance of the subloop and overall performance. A systematic analysis of the variation between the overall performance and the sub cycle is beneficial to obtaining the practical application potential of the cycle. Based on the variation characteristics of the multisource energy of the engine, the loop cycle and overall waste heat recovery potential are systematically evaluated from the perspectives of net output power, heat transfer area, power output of per unit heat transfer area (POPA), exergy destruction, and emissions of CO_2 equivalent (ECE). Under operation characteristics in cycle, the variation laws of thermodynamic index, heat transfer index, thermoeconomic index, and environmental impact of loop are analyzed. The analysis of nonlinear response characteristics is of significance to improve the overall fuel utilization. On the basis of the key operating parameters in a cycle, the multiple variables synergistic effects on the performance are analyzed. In this study, the comprehensive index assessment for DORC under a changeable environment can offer a reference for the application possibility of DORC.

2. Description of DORC

Figure 1 shows the thermodynamic cycle of DORC. Figure 1a shows DORC topology. In the evaporator, the exhaust after passing through the turbine exchanges energy with fluid. The fluid in the HT cycle becomes vapor, and then enters the expander. Figure 1b is the temperature-entropy of the HT cycle. The exhausted after work of HT cycle, intercooler and coolant are used as heat source for LT cycle. Figure 1c is LT cycle temperature-entropy. R245fa is widely used in the field of ORC therefore R245fa is selected in this paper [29–31].

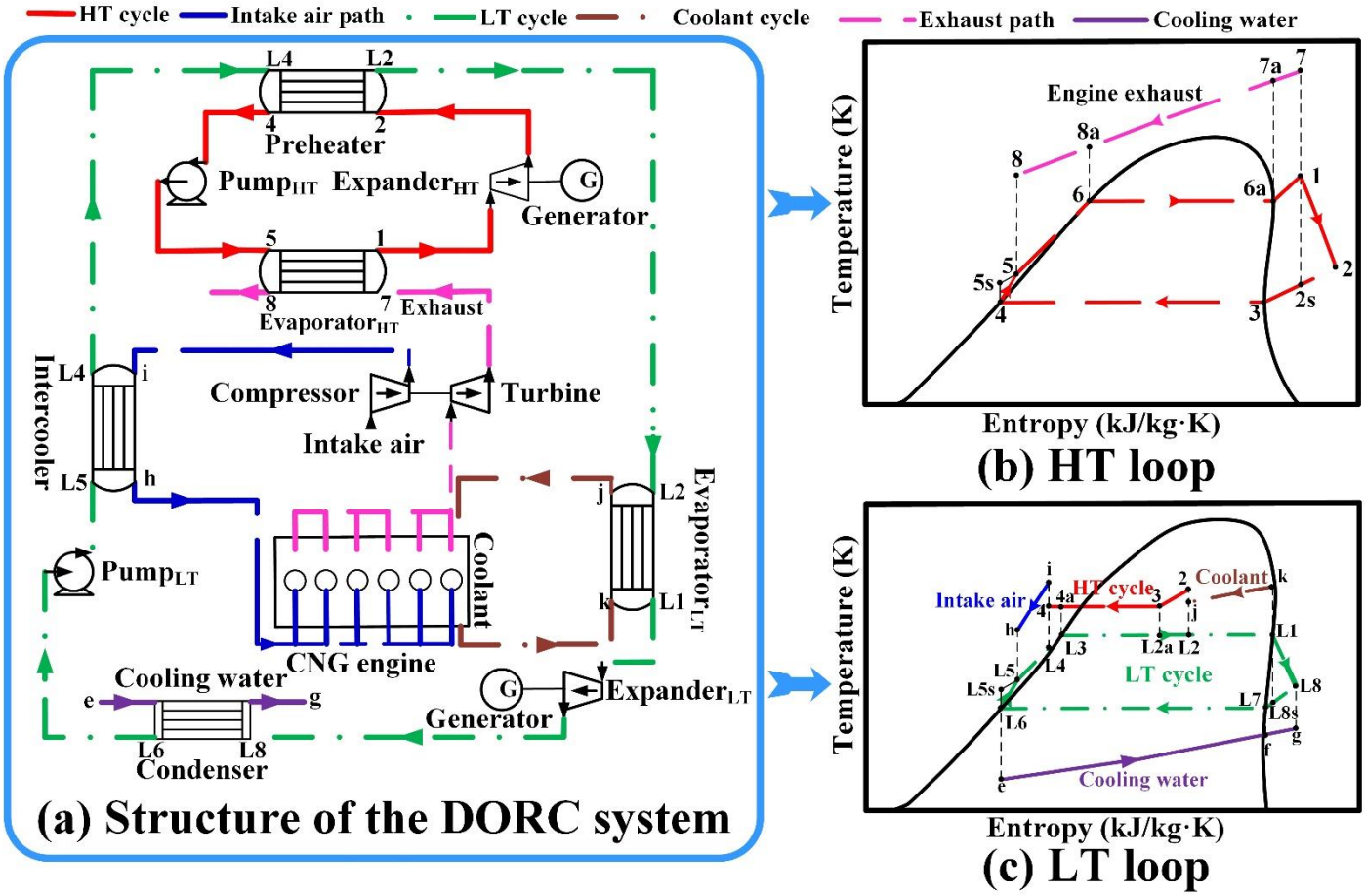

Figure 1. Topology and thermodynamic cycle of DORC. (**a**) structure of the DORC system. (**b**) HT loop. (**c**) LT loop.

3. Construction of Mathematical Model

For an expander, we choose the inlet temperature and pressure. For a condenser, we choose the inlet temperature. The parameters mentioned above are chosen as the input variables. The pinch point temperature difference in the evaporator and condenser is 5 K and 10 K, respectively [32].

3.1. Thermal Balance Model

During the operation of CNG engines, energy converted into useful work is only one part; the other part is energy lost with the dissipation of waste heat. Table 3 shows the technical parameters of the CNG engine.

Table 3. Technical parameters of CNG engines.

Parameters	Units	Values
Stroke and bore	mm	114 × 144
Maximum torque	Nm	1120
Displacement	L	8.9
Cylinder number	-	6

The construction process is as follows:

$$\dot{Q}_{exh} + \dot{W}_{eng} + \dot{Q}_{cool} + \dot{Q}_{inter} + \dot{Q}_{other} = \dot{Q}_{tot} \quad (1)$$

$$\dot{Q}_{inter} = \dot{m}_{inter} C_{p_{air}} (T_{inter,in} - T_{inter,out}) \quad (2)$$

$$\dot{Q}_{\text{cool}} = \dot{m}_{\text{cool}} C_{p_{\text{cool}}} (T_{\text{cool,in}} - T_{\text{cool,out}}) \tag{3}$$

$$\dot{Q}_{\text{exh}} = \dot{m}_{\text{fuel}} H \tag{4}$$

3.2. Thermodynamic Model

The thermodynamic model construction process of the HT cycle is as follows:
(1) Expansion process:
Power output:

$$\dot{W}_{\text{exp,HT}} = \dot{m}_{\text{wf,HT}} (h_1 - h_2) \tag{5}$$

Isentropic efficiency:

$$\eta_{\text{exp,HT}} = \frac{h_1 - h_2}{h_1 - h_{2\text{s}}} \tag{6}$$

(2) Pressurization process:
Power consumption of working medium pump:

$$\dot{W}_{\text{p,HT}} = \dot{m}_{\text{wf,HT}} (h_5 - h_4) \tag{7}$$

Isentropic efficiency:

$$\eta_{\text{p,HT}} = \frac{h_{5\text{s}} - h_4}{h_5 - h_4} \tag{8}$$

(3) Condensation process:

$$\dot{Q}_{\text{pre,HT}} = \dot{m}_{\text{wf,HT}} (h_2 - h_4) \tag{9}$$

(4) Evaporation process:

$$\dot{Q}_{\text{eva,HT}} = \dot{m}_{\text{wf,HT}} (h_1 - h_5) = \dot{m}_{\text{exh}} (h_7 - h_8) \tag{10}$$

The power is:

$$\dot{W}_{\text{net,HT}} = \dot{W}_{\text{exp,HT}} - \dot{W}_{\text{p,HT}} \tag{11}$$

The thermodynamic model construction process of LT cycle is as follows:
(1) Expansion process:
Power output:

$$\dot{W}_{\text{exp,LT}} = \dot{m}_{\text{wf,LT}} (h_{\text{L1}} - h_{\text{L8}}) \tag{12}$$

Isentropic efficiency:

$$\eta_{\text{exp,LT}} = \frac{h_{\text{L1}} - h_{\text{L8}}}{h_{\text{L1}} - h_{\text{L8s}}} \tag{13}$$

(2) Pressurization process:
Power is:

$$\dot{W}_{\text{p,LT}} = \dot{m}_{\text{wf,LT}} (h_{\text{L5}} - h_{\text{L6}}) \tag{14}$$

Isentropic efficiency:

$$\eta_{\text{p,LT}} = \frac{h_{\text{L5s}} - h_{\text{L6}}}{h_{\text{L5}} - h_{\text{L6}}} \tag{15}$$

(3) Condensation process:

$$\dot{Q}_{\text{con,LT}} = \dot{m}_{\text{wf,LT}} (h_{\text{L8}} - h_{\text{L6}}) \tag{16}$$

(4) Evaporation process:

$$\dot{Q}_{\text{pre,LT}} = \dot{m}_{\text{wf,LT}} (h_{\text{L2}} - h_{\text{L4}}) \tag{17}$$

$$\dot{Q}_{\mathrm{eva,LT}} = \dot{m}_{\mathrm{wf,LT}}(h_{\mathrm{L1}} - h_{\mathrm{L2}}) \tag{18}$$

Power is:

$$\dot{W}_{\mathrm{exp,LT}} = \dot{m}_{\mathrm{wf,LT}}(h_{\mathrm{L1}} - h_{\mathrm{L8}}) \tag{19}$$

The DORC power can be expressed as:

$$\dot{W}_{\mathrm{net}} = \dot{W}_{\mathrm{net,HT}} + \dot{W}_{\mathrm{net,LT}} \tag{20}$$

The system thermal efficiency can be expressed as:

$$\eta_{\mathrm{th}} = 100\% \times \frac{\dot{W}_{\mathrm{net}}}{\dot{Q}_{\mathrm{eva,HT}} + \dot{Q}_{\mathrm{int}} + \dot{Q}_{\mathrm{eva,LT}}} \tag{21}$$

3.3. Heat Transfer and Thermoeconomic Model

DORC involves multiple heat transfer processes in the process of thermal power conversion. The heat exchanger in the HT cycle is a fin-and-tube evaporator. The remaining heat exchangers in the system are plate heat exchangers [33–35]. The evaporation process can be divided into preheating, two-phase and superheating. The condensation process is divided into preheating, two-phase, superheating and condensation [36,37]. Table 4 shows the parameters of the heat exchanger.

Table 4. Exchangers parameters.

Parameters	Units	Values
Plate heat exchanger		
Plate width	m	0.123
Plate thickness	mm	0.35
Corrugation depth	mm	3
Fin-and-tube heat exchanger		
Fin height	mm	12
Tube pitch	mm	60
Row pitch	mm	100

According to the logarithmic mean temperature difference (LMTD), the heat transfer rate can be expressed as [38–40]:

$$\dot{Q} = AK\Delta T_{\mathrm{LMTD}} \tag{22}$$

$$\Delta T_{\mathrm{LMTD}} = \frac{\Delta t_{\max} - \Delta t_{\min}}{\mathrm{In}\frac{\Delta t_{\max}}{\Delta t_{\min}}} \tag{23}$$

The overall heat transfer coefficient is:

$$\frac{1}{K_{\mathrm{ft}}} = \frac{\beta}{\alpha_{\mathrm{in}}} + r_{\mathrm{in}}\beta + \frac{\delta\beta}{\lambda} + \frac{r_{\mathrm{out}}}{\eta_{\mathrm{f}}} + \frac{1}{\alpha_{\mathrm{out}}\eta_{\mathrm{f}}} \tag{24}$$

$$\alpha = \frac{\lambda Nu}{d} \tag{25}$$

Based on Zhukauskas correlation, the Nusselt number can be expressed as [41]:

$$Nu_{\mathrm{exh}} = 0.35\varepsilon^{0.2} Re_{\mathrm{exh}}^{0.6} Pr_{\mathrm{exh}}^{0.36} \left(\frac{Pr_{\mathrm{exh}}}{Pr_{\mathrm{exh,w}}}\right) \quad (1000 < Re < 2 \times 105) \tag{26}$$

$$Nu_{\mathrm{exh}} = 0.71 Re_{\mathrm{exh}}^{0.5} Pr_{\mathrm{exh}}^{0.36} \left(\frac{Pr_{\mathrm{exh}}}{Pr_{\mathrm{exh,w}}}\right)^{0.25} \quad (Re < 1000) \tag{27}$$

Based on the Gnielinski correlation, the heat transfer coefficients of the preheating zone and superheating zone can be expressed as [42]:

$$Nu_{\mathrm{wf}} = \frac{d\alpha}{\lambda} = \frac{(f/8)(Re_{\mathrm{wf}} - 1000)Pr_{\mathrm{wf}}}{1 + 12.7\sqrt{f/8}\left(Pr_{\mathrm{wf}}^{2/3} - 1\right)}\left[1 + \left(\frac{d}{l}\right)^{2/3}\right]c_{\mathrm{t}} \tag{28}$$

Based on the Filonenko correlation, the Darcy drag coefficient can be expressed as:

$$f = \left(1.82\log_{10} Re_{\mathrm{wf}} - 1.64\right)^{-2} \tag{29}$$

Preheat zone:

$$c_{\mathrm{t}} = \left(\frac{Pr_{\mathrm{wf}}}{Pr_{\mathrm{w}}}\right)^{0.01} \tag{30}$$

among them, $\frac{Pr_{\mathrm{wf}}}{Pr_{\mathrm{w}}} = 0.05 \sim 20$.

Superheat zone:

$$c_{\mathrm{t}} = \left(\frac{T_{\mathrm{wf}}}{T_{\mathrm{w}}}\right)^{0.45} \tag{31}$$

among them, $\frac{T_{\mathrm{wf}}}{T_{\mathrm{w}}} = 0.5 \sim 1.5$.

Based on Liu-Winterton correlation, the heat transfer coefficient of two-phase zone is [43]:

$$\alpha_{\mathrm{tp}} = \sqrt{(F\alpha_{\mathrm{fb}})^2 + (S\alpha_{\mathrm{nb}})^2} \tag{32}$$

$$S = \left(1 + 0.055F^{0.1}\mathrm{Re}_{\mathrm{l,i}}^{0.16}\right)^{-1} \tag{33}$$

$$F = \left(1 + xPr_1\left(\frac{\rho_1}{\rho_{\mathrm{v}}} - 1\right)\right)^{0.35} \tag{34}$$

among them, $2.95 < \mathrm{d} < 32$ mm; $568.9 < \mathrm{Re} < 8.75 \times 10^5$.

Based on Dittus-Boelter correlation, the film boiling heat transfer coefficient can be expressed as [44]:

$$\alpha_{\mathrm{fb}} = 0.023(\lambda_1/d)\mathrm{Re}_{\mathrm{l,i}}^{0.8}\mathrm{Pr}_{\mathrm{l}}^{0.4} \tag{35}$$

Based on the Copper correlation formula, the heat transfer coefficient of nucleated boiling can be expressed as:

$$\alpha_{\mathrm{nb}} = 55p_{\mathrm{r}}^{0.12}q_{\mathrm{w}}^{2/3}\left(-\log_{10} p_r\right)^{-0.55}M^{-0.5} \tag{36}$$

The overall heat transfer coefficient can be expressed as [45–47]:

$$\frac{1}{K_{\mathrm{pl}}} = \frac{\beta}{\alpha_{\mathrm{in}}} + r_{\mathrm{in}} + \frac{\delta}{\lambda} + r_{\mathrm{out}} + \frac{1}{\alpha_{\mathrm{out}}} \tag{37}$$

Based on the Chisholm-Wanniarachchi correlation, the heat transfer coefficients of preheating zone and superheating zone can be expressed as [48]:

$$Nu = \frac{d\alpha}{\lambda} = 0.724\left(\frac{6\beta}{\pi}\right)^{0.646} Re^{0.583}Pr^{1/3} \tag{38}$$

$$Re = \frac{Gd_{\mathrm{h}}}{\mu_1}\left(G = \frac{\dot{m}}{Nwb};\ d_{\mathrm{h}} = \frac{4wb}{2(w+b)}\right) \tag{39}$$

Based on the Yan-Lin correlation:

$$Nu = \frac{d\alpha_{\mathrm{tp}}}{\lambda} = 1.926\mathrm{Pr}_{\mathrm{l}}^{1/3}Bo_{\mathrm{eq}}^{0.3}Re_{\mathrm{eq}}^{0.5}\left[1 - x_{\mathrm{i}} + x_{\mathrm{i}}\left(\frac{\rho_{\mathrm{l}}}{\rho_{\mathrm{v}}}\right)^{0.5}\right] \tag{40}$$

$$Re_{eq} = \frac{G_{eq} d_h}{\mu_1}\left(G_{eq} = G\left[1 - x_i + x_i\left(\frac{\rho_l}{\rho_v}\right)^{0.5}\right]\right);\ Bo_{eq} = \frac{q}{G_{eq} r_{fg}} \tag{41}$$

The heat transfer coefficient of the condensation zone can be expressed as:

$$\alpha = 4.118\left(\frac{\lambda}{d_h}\right) Re_{eq}^{0.4} Pr^{1/3} \tag{42}$$

POPA can evaluate the thermoeconomic performance of DORC. POPA can be expressed as [49,50]:

$$\text{POPA} = \frac{\dot{W}_{net}}{A} \tag{43}$$

3.4. Exergy Destruction Model

The exergy destruction model construction process of the HT cycle is as follows:
(1) Expansion process:

$$\dot{I}_{exp,HT} = T_{env}\dot{m}_{wf,HT}(s_2 - s_1) \tag{44}$$

(2) Pressurization process:

$$\dot{I}_{p,HT} = T_{env}\dot{m}_{wf,HT}(s_5 - s_4) \tag{45}$$

(3) Condensation process:

$$\dot{I}_{pre,HT} = T_{env}\dot{m}_{wf,HT}(s_4 - s_2) + T_{env}\dot{m}_{wf,LT}(s_{L2} - s_{L4}) \tag{46}$$

(4) Evaporation process:

$$\dot{I}_{eva,HT} = T_{env}\dot{m}_{wf,HT}\left[(s_1 - s_5) - \frac{h_1 - h_5}{T_{HT}}\right] \tag{47}$$

$$T_{HT} = T_1 + \Delta T_{HT} \tag{48}$$

$$\Delta T_{HT} = \frac{(T_7 - T_1) - (T_8 - T_5)}{\ln\frac{T_7 - T_1}{T_8 - T_5}} \tag{49}$$

The exergy destruction model construction process of the LT cycle is as follows:
(1) Expansion process:

$$\dot{I}_{exp,LT} = T_{env}\dot{m}_{wf,LT}(s_{L8} - s_{L1}) \tag{50}$$

(2) Pressurization process:

$$\dot{I}_{p,LT} = T_{env}\dot{m}_{wf,LT}(s_{L5} - s_{L6}) \tag{51}$$

(3) Condensation process:

$$\dot{I}_{con,LT} = T_{env}\dot{m}_{wf,LT}\left[(s_{L6} - s_{L8}) - \frac{h_{L6} - h_{L8}}{T_{LT}}\right] \tag{52}$$

$$T_{LT} = T_{L6} - \Delta T_{LT} \tag{53}$$

$$\Delta T_{LT} = \frac{(T_{L8} - T_g) - (T_{L6} - T_e)}{\ln\frac{T_{L8} - T_g}{T_{L6} - T_e}} \tag{54}$$

(4) Evaporation process:

$$\dot{I}_{\text{inter}} = T_{\text{env}}\dot{m}_{\text{wf,LT}}\left[(s_{\text{L4}} - s_{\text{L5}}) - \frac{h_{\text{L4}} - h_{\text{L5}}}{T_{\text{inter}}}\right] \tag{55}$$

$$T_{\text{inter}} = T_{\text{L4}} + \Delta T_{\text{inter}} \tag{56}$$

$$\Delta T_{\text{inter}} = \frac{(T_{\text{i}} - T_{\text{L4}}) - (T_{\text{h}} - T_{\text{L5}})}{In\frac{T_{\text{i}} - T_{\text{L4}}}{T_{\text{h}} - T_{\text{L5}}}} \tag{57}$$

$$\dot{I}_{\text{eva,LT}} = T_{\text{env}}\dot{m}_{\text{wf,LT}}\left[(s_{\text{L1}} - s_{\text{L2}}) - \frac{h_{\text{L1}} - h_{\text{L2}}}{T_{\text{cool}}}\right] \tag{58}$$

$$T_{\text{cool}} = T_{\text{L1}} + \Delta T_{\text{cool}} \tag{59}$$

$$\Delta T_{\text{cool}} = \frac{(T_{\text{k}} - T_{\text{L1}}) - (T_{\text{j}} - T_{\text{L2}})}{\text{In}\frac{T_{\text{k}} - T_{\text{L1}}}{T_{\text{j}} - T_{\text{L2}}}} \tag{60}$$

DORC total exergy destruction can be expressed as:

$$\dot{I}_{\text{tot}} = \dot{I}_{\text{exp,HT}} + \dot{I}_{\text{pre,HT}} + \dot{I}_{\text{p,HT}} + \dot{I}_{\text{eva,HT}} + \dot{I}_{\text{exp,LT}} + \dot{I}_{\text{con,LT}} + \dot{I}_{\text{p,LT}} + \dot{I}_{\text{inter}} + \dot{I}_{\text{eva,LT}} \tag{61}$$

3.5. Environmental Impact Model

Select the emissions of CO_2 equivalent (ECE) to assess environmental impact [51–53]. ECE can be expressed as [54,55]:

$$\text{ECE} = \text{Direct emissions} + \text{Indirect emissions} \tag{62}$$

$$\text{Direct emissions} = FC \times (LT \times ALR + EOL) \times GWP \tag{63}$$

$$\begin{aligned}\text{Indirect emissions} = {} & LT + AEC \times CE + m \times CM + mr \times CMR \\ & + (FC + LT \times ALR + FC) \times CFM + FC \times (1 - EOL) \times CFR\end{aligned} \tag{64}$$

Among them, *FC* is the charge; *ALR* is the annual leakage rate; *EOL* is the end-of-life loss rate; *GWP* is global warming potential; *LT* is the system lifetime; *AEC* is annual energy consumption; *CE* is the CO_2,eq produced by unit energy consumption; *m* is the mass of material; *CM* is the CO_2,eq produced unit material mass; *mr* is the mass of recycled material; *CMR* is the CO_2,eq produced unit recycled material mass. *CFM* is the eq produced of working fluid manufacturing of carbon dioxide equivalent. *CFR* is the CO_2, eq produced of working fluid disposal.

The charge amount can be expressed as:

$$FC = 5.57\dot{W}_{\text{net}} \tag{65}$$

The amount of steel consumed by the expander is:

$$m_{\text{steel,exp}} = 31.227\dot{W}_{\text{exp}} \tag{66}$$

The amount of steel consumed by the working fluid pump is:

$$m_{\text{steel,p}} = 14\dot{W}_{p} \tag{67}$$

3.6. Validation

Compared with Refs. [56–59], the relative errors of power are 0.37%, 0.39%, 3.49%, and 4.82%, respectively. The relative error of the heat exchange area is 0.62%, 1.58%, 6.99% and 3.48%, respectively.

4. Results and Discussion

4.1. Waste Heat Characteristics of CNG Engine

4.1.1. Intercooler

Figure 2 is characteristic of an intercooler in variable conditions. Figure 2a presents the variation trends of inlet temperature. With the increasing of intake mass flow rate, the inlet temperature gradually increases. When the flow rate reaches about 0.15 kg/s, the increasing trend of inlet temperature gradually slows down. With the increasing of intake mass flow rate, the nonlinear variation trend between inlet temperature and speed becomes evident. Compared with the speed, the inlet mass flow rate exerts a greater impact on the inlet temperature. Figure 2b presents variation trends of the temperature difference. With the increasing of intake mass flow rate, the temperature difference gradually increases. Before 0.18 kg/s, the increasing trend of temperature difference gradually slows down. From approximately 0.2 kg/s, the increasing trend of temperature difference gradually becomes evident. With the increasing of speed, the temperature difference gradually increases. With the increasing of intake mass flow rate, the nonlinear variation trend between temperature difference and speed gradually becomes evident. Compared with speed, the intake mass flow rate has a greater influence on the temperature difference.

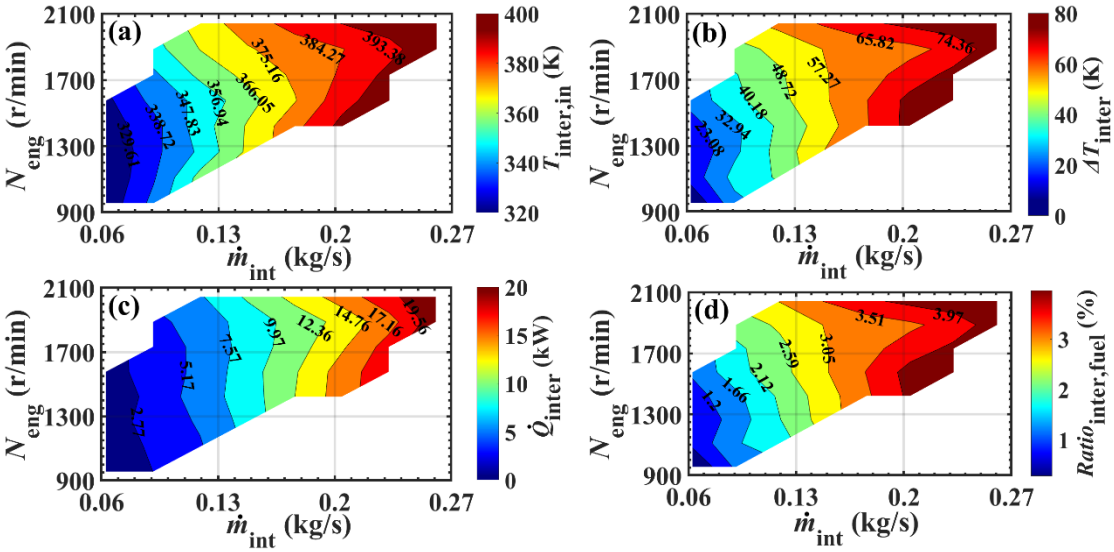

Figure 2. Waste heat characteristics of intercooler in variable working environments. (**a**) Inlet temperature of intercooler. (**b**) Temperature different of intercooler. (**c**) Heat transfer rate of intercooler. (**d**) Proportion of heat transfer rate in intercooler.

Figure 2c presents the variation trends of heat transfer rate. With the increasing of intake flow, the rate rises gradually, and the increasing trend of the heat transfer rate becomes more evident. With the increasing of speed, the rate gradually increases. With the increasing of intake mass flow rate, the nonlinear variation trend between the heat transfer rate and speed gradually becomes evident. Compared with speed, the intake mass flow rate exerts a greater effect on the rate. The proportion is shown in Figure 2d. With the increasing of the intake mass flow rate, the ratio gradually increases. Before 0.18 kg/s, the increasing trend of the ration gradually slows down. From approximately 0.2 kg/s, the trend of increasing proportion becomes more evident. With the increasing of speed, the proportion increases gradually. With the increasing of intake mass flow rate, the nonlinear change trend between the proportion and the speed gradually becomes evident. Compared with speed, the intake flow exerts a greater influence on the proportion.

4.1.2. Coolant

Figure 3 presents the characteristics of a coolant with the variable operating environment. Among them, Figure 3a presents the variation characteristics of inlet temperature. With the increasing of intake flow, temperature first increases and then decreases. Around 0.09–0.12 kg/s, the inlet temperature reaches the maximum. As the speed increases, the correlation of the mentioned parameters first increases and then decreases. With the increasing of speed, temperature rises first and then drops. Compared with the intake mass flow rate, the speed exerts more of an influence on the inlet temperature. Figure 3b presents the variation characteristics of temperature difference. With the increasing of intake mass flow rate, the temperature difference gradually increases. Before 0.09 kg/s, the temperature difference gradually decreases with the increasing of speed. When reaches 0.09–0.18 kg/s, with speed increasing, temperature difference drops first and then rises. From approximately 0.18 kg/s, temperature difference gradually increases. Compared to intake mass flow rate, the speed exerts more influence on the temperature difference.

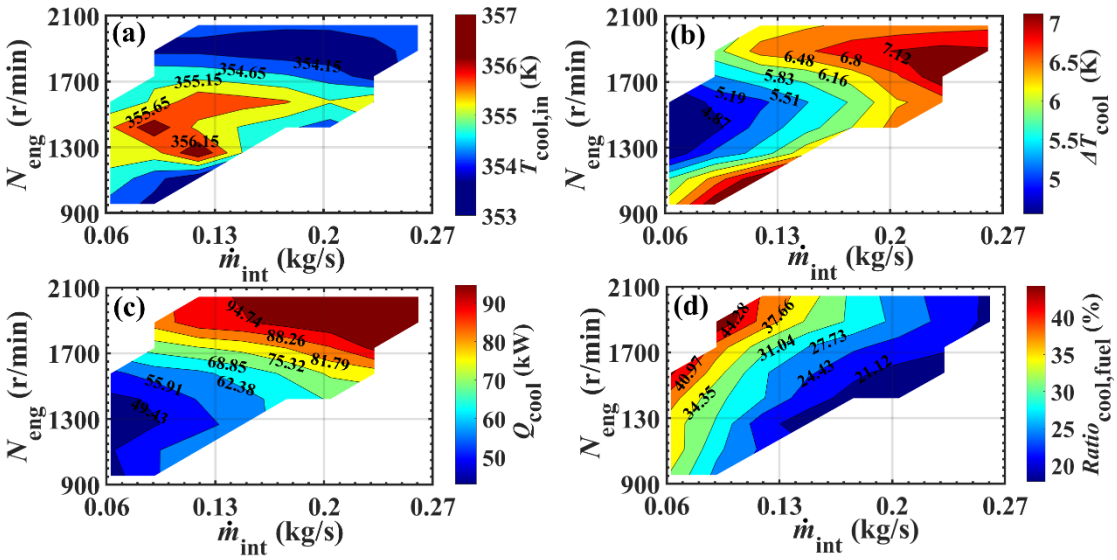

Figure 3. Waste heat characteristics of coolant in variable working environments. (**a**) Inlet temperature of coolant. (**b**) Temperature different of coolant. (**c**) Heat transfer rate of coolant. (**d**) Proportion of heat transfer rate in coolant.

Figure 3c presents the variation characteristics of the heat transfer rate. Accompanied with an increase in intake flow, the rate increases gradually. From around 1700 r/min, the increasing trend has moderated. Then, with the increasing of the speed, the heat transfer rate gradually increases. From around 0.13 kg/s, with the increasing of the speed, trend gradually becomes evident. Compared with the intake mass flow rate, the speed exerts a greater impact on rate. Figure 3d presents the heat transfer rate proportion. With the increasing of intake flow, the proportion drops. Moreover, the trend of increasing the proportion gradually slows down. With the increasing of intake flow, the trend slows down. Compared with intake mass flow rate, the speed exerts more influence on the proportion.

4.1.3. Exhaust

Figure 4 presents the characteristics of the variable working conditions exhaust waste heat. Figure 4a presents the exhaust temperature of the variation characteristics. Before 1200 r/min, with the increasing of intake mass flow rate, there is an increase in the exhaust temperature. From around 1200 r/min, however, the increasing trend mentioned above slows down. From around 1700 r/min, the change of intake mass flow rate has a minimal effect on exhaust temperature. Figure 4b presents the variation characteristics of exhaust back pressure. With the increasing of speed, there is generally a trend of increasing on

the exhaust back pressure. The increasing of intake mass flow rate makes the relationship between the speed and exhaust back pressure gradually become evident. Compared with the speed, the intake mass flow rate exerts greater influence on the exhaust back pressure.

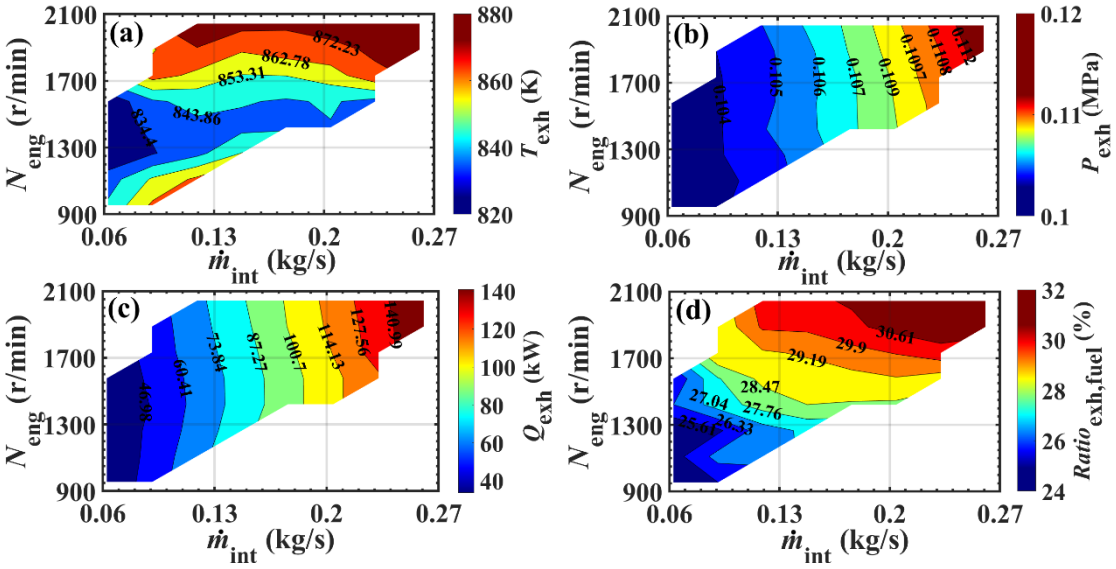

Figure 4. Waste heat characteristics of exhaust in variable working environments. (**a**) Inlet temperature of exhaust. (**b**) Temperature different of exhaust. (**c**) Heat transfer rate of exhaust. (**d**) Proportion of heat transfer rate in exhaust.

Figure 4c presents the heat transfer rate variation characteristics. Accompanied by the increasing of the intake mass flow rate, the rate gradually increases. With an increase in speed, the rate generally shows a gradually increasing trend. The increasing of intake flow makes the correlation between speed and heat transfer rate more pronounced. Compared with speed, the intake mass flow rate exerts more of an effect on the heat transfer rate. Figure 4d shows the proportion of the heat transfer rate. Before 1600 r/min, the proportion gradually increases as the intake mass flow rate increases. From around 1600 r/min, the trend of increasing proportion slows down. With the increase in rotational speed, the proportion increases gradually. The correlation between rotational speed and proportion considerably increases with the intake mass flow rate increase.

4.2. Power Analysis

4.2.1. Variable Working Conditions

Figure 5 presents the power characteristic analysis of the HT cycle and LT cycle under variable system working conditions. Figure 5a is the power characteristic analysis. With the increasing of the intake mass flow rate, both the HT and LT cycles' power gradually increases. The maximum value of the HT and LT powers are 15.82 and 20.6 kW, respectively. Compared with the speed, the intake mass flow rate has more of an effect on the power of the loop. Figure 5b is the power characteristic analysis in the system. The system power gradually increases. The maximum system power is 36.42 kW. Compared with speed, intake mass flow rate has a more significant impact on system power.

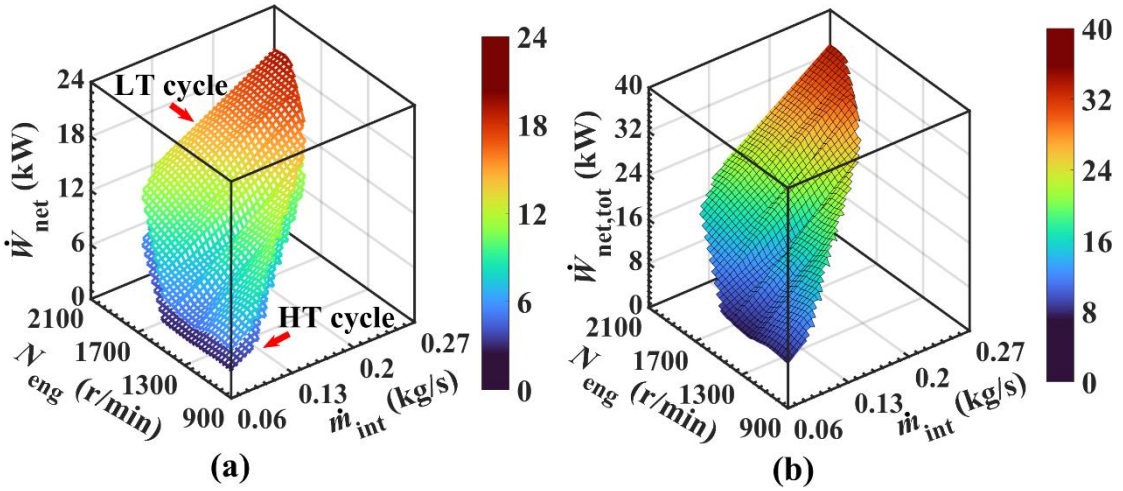

Figure 5. Power output of HT cycle, LT cycle and system in variable working environments. (**a**) Power characteristic. (**b**) power characteristic in the system.

4.2.2. Key Variables

Figure 6 shows the power influence characteristics of key operating parameters on the HT and LT cycles. Among them, Figure 6a presents the influence characteristics of different loop condenser inlet temperatures on HT cycle power. To HT cycle, with the condenser inlet temperature increases, the power gradually decreases. With the LT cycle, the condenser inlet temperature increases, while the power impact to the HT cycle is slight. Compared with the condenser inlet temperature, the temperature change exerts less influence on the power of the HT cycle. Figure 6b shows the impact characteristics inlet temperature and the pressure of the expander on the power in the HT cycle.

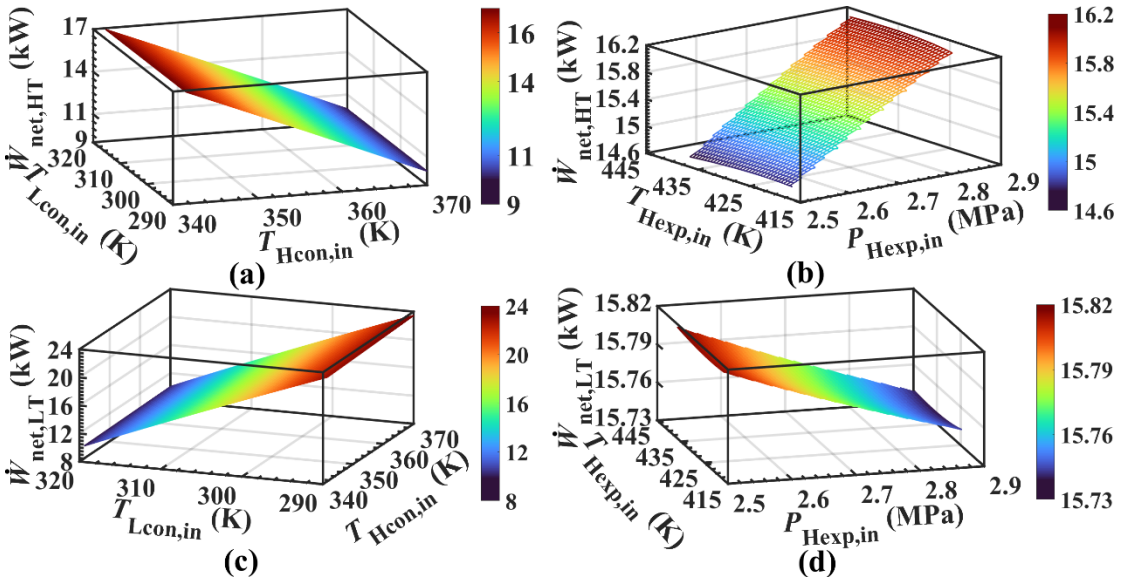

Figure 6. Influence characteristics of key variables on power in HT cycle and LT cycle. (**a**) Influence characteristics of different loop condenser inlet temperatures on HT cycle power. (**b**) Impact characteristics inlet temperature and the pressure of the expander on the power in the HT cycle. (**c**) Effect characteristics of different loop condenser inlet temperatures on LT cycle power. (**d**) Effect of expander parameters of the HT cycle on the power of the LT cycle.

Figure 6c shows the effect characteristics of different loop condenser inlet temperatures on LT cycle power. The power of the LT cycle gradually decreases. Compared with the

condenser inlet temperature in the LT cycle, the change of condenser inlet temperature in the HT cycle has less influence on the power of the LT cycle. Figure 6d presents the effect of expander parameters of the HT cycle on the power of the LT cycle. As the inlet pressure of the HT cycle increases, the power of the LT cycle gradually decreases. The change of inlet temperature of the expander in the HT cycle has little influence on the power of the LT cycle.

Figure 7 shows the effect characteristics of system power. Figure 7a presents the effect characteristics of inlet temperature of a condenser on the system power in a different cycle. As the inlet temperature in condenser increases in the HT cycle, the power gradually decreases. As condenser inlet temperature of the LT cycle increases, system power gradually decreases. Compared to condenser inlet temperature of the HT cycle, the inlet temperature of the condenser in the LT cycle has a better effect on system power. Figure 7b shows effect characteristics of parameter of expander on system power in HT cycle. As inlet expander pressure increases, system power gradually increases. As the temperature of the inlet increases, the system power does not change significantly.

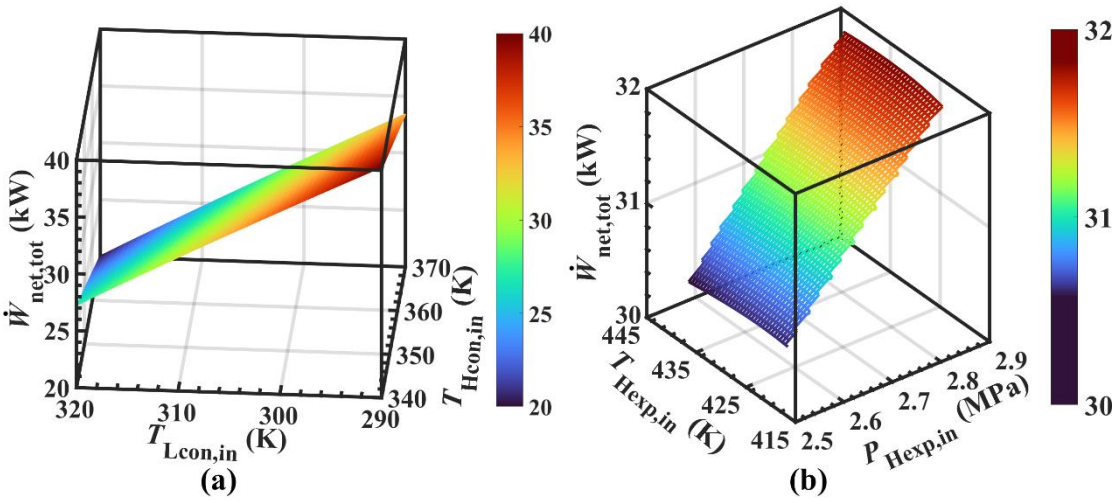

Figure 7. Influence characteristics of key variables on system power output. (**a**) Effect characteristics of inlet temperature of a condenser on the system power in a different cycle. (**b**) Effect characteristics of parameter of expander on system power in HT cycle.

4.3. Heat Transfer Surface Analysis

4.3.1. Variable Working Conditions

Figure 8 shows the analysis of heat transfer surface characteristics of the HT cycle, LT cycle and system under variable working environments. Figure 8a shows the analysis of heat transfer surface for different loops. With the increase of speed, heat transfer surface of different loops gradually decreased. Maximum heat transfer surface is 12.56 m^2 and 10.78 m^2, respectively. Compared with speed, the intake mass flow rate has a better impact on heat transfer surface of the loop. Figure 8b shows the characteristic analysis in the system heat transfer surface. As the intake mass flow rate increases, the heat transfer surface increases gradually. The maximum system heat transfer surface is 23.34 m^2. The intake mass flow rate has a better impact on the system heat transfer surface.

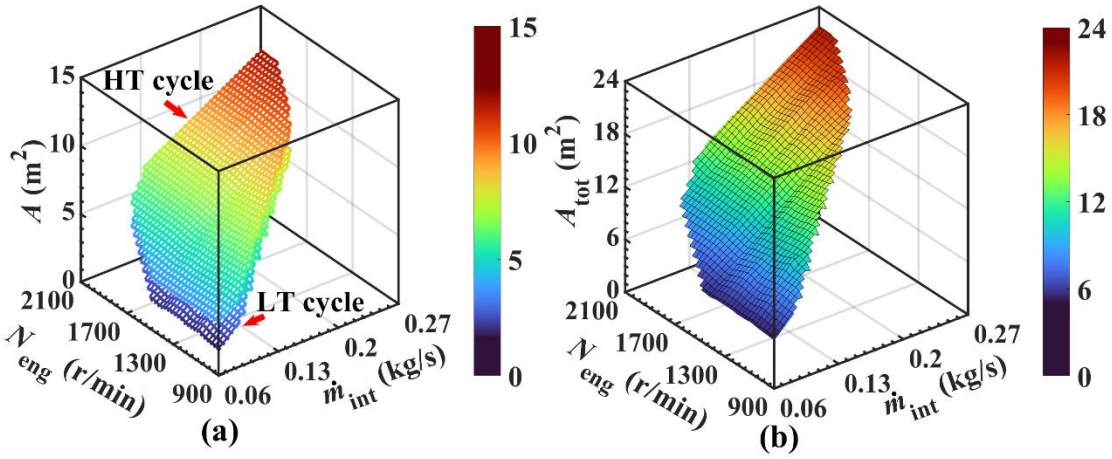

Figure 8. Heat transfer surface of HT cycle, LT cycle and system under variable working conditions. (**a**) Heat transfer surface for different loops. (**b**) System heat transfer surface.

4.3.2. Key Variables

Figure 9 shows the effect of the heat transfer surface in the HT cycle and the LT cycle. Figure 9a shows effect the characteristics in the condenser inlet temperature of different loops on the heat transfer surface for the HT cycle. As the inlet temperature increases, the trend of the surface increase gradually becomes obvious. As the condenser inlet temperature increases in the LT cycle, the heat transfer surface of the HT cycle changes little. The change of the condenser inlet temperature in the LT cycle has less of an effect on the surface in the HT cycle. Figure 9b shows the effect characteristics of heat transfer surface in the HT cycle. The heat transfer surface in the HT cycle decreases gradually. The change of inlet temperature of the expander in the HT cycle has less influence on the heat transfer surface of the HT cycle.

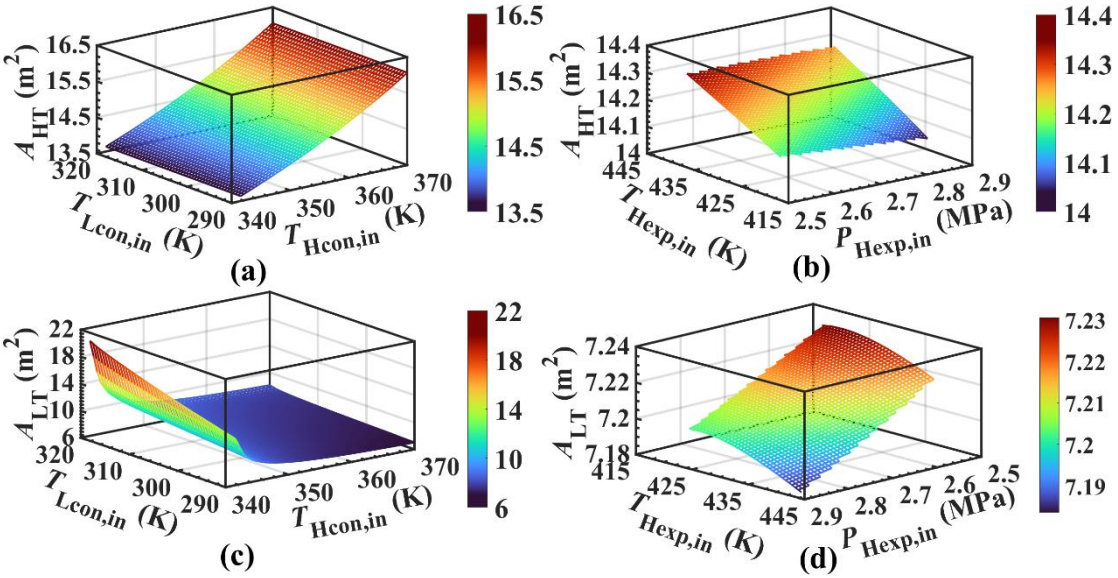

Figure 9. Influence characteristics of key variables on the heat transfer surface of the HT cycle and the LT cycle. (**a**) Effect the characteristics in the condenser inlet temperature of different loops on the heat transfer surface for the HT cycle. (**b**) Effect characteristics of heat transfer surface in the HT cycle. (**c**) Effect characteristics in different loops on the heat transfer surface of the LT cycle. (**d**) Effect characteristics of the heat transfer surface of the LT cycle.

Figure 9c shows the effect characteristics in different loops on the heat transfer surface of the LT cycle. The surface of the LT cycle gradually decreases. Moreover, the variation trend gradually slowed down. As the condenser inlet temperature increases in the LT cycle, the surface gradually increases. The change of the condenser inlet temperature in the LT cycle has less influence on the heat transfer surface of the LT cycle. Figure 9d shows the effect characteristics of the heat transfer surface of the LT cycle. The surface of the LT cycle increases gradually. With the increase of expander inlet temperature in the HT cycle, the surface of the LT cycle gradually increases. The change of heat transfer surface in the HT cycle has less effect on the heat transfer surface of the LT cycle.

Figure 10 shows the effect characteristics of the system heat transfer surface. Figure 10a shows the effect characteristics of inlet temperature in a condenser on the system heat transfer surface in the HT cycle and the LT cycle. As the condenser inlet temperature increases for the HT cycle, the surface gradually decreases. Compared with the condenser inlet temperature in the LT cycle, the condenser inlet temperature in the HT cycle has a better effect on the surface of the system. Figure 10b shows the effect characteristics of the parameters of the expander in the HT cycle on the system heat transfer surface. As the expander inlet pressure increases during the HT cycle, the heat transfer surface of the system decreases gradually.

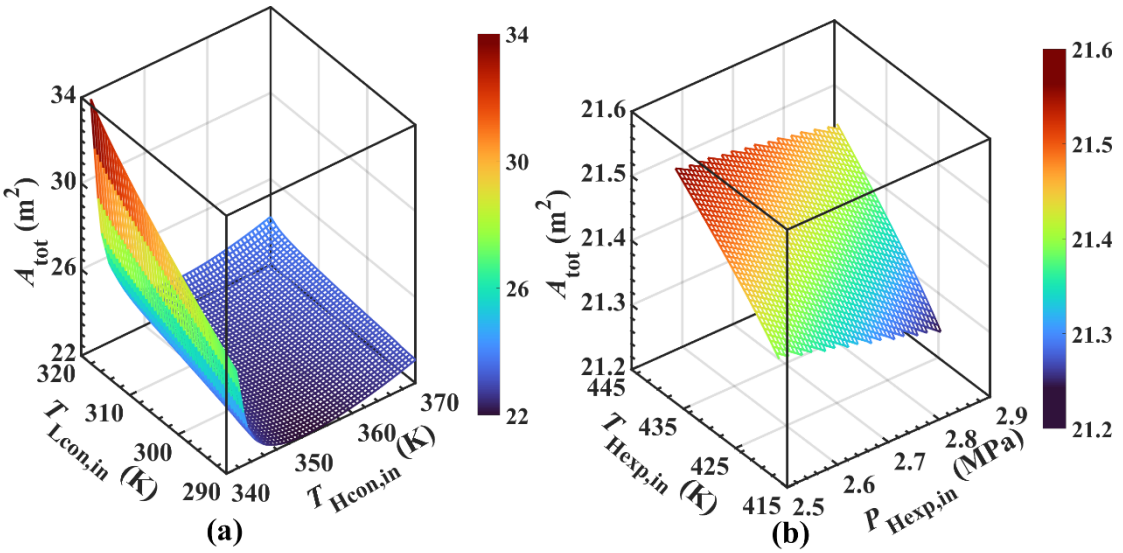

Figure 10. Influence characteristics of key variables on the system heat transfer surface. (**a**) Effect characteristics of inlet temperature in a condenser on the system heat transfer surface in the HT cycle and the LT cycle. (**b**) Effect characteristics of the parameters of the expander in the HT cycle on the system heat transfer surface.

4.4. POPA

4.4.1. Variable Working Conditions

Figure 11 shows the POPA characteristics analysis of the HT cycle, LT cycle and the system under variable working conditions. Figure 11a shows the POPA characteristics analysis of different cycles. The maximum POPA of the HT cycle is 1.26 kW/m^2. With the increase of speed, the POPA of the LT cycle generally showed an increasing trend. The change of POPA is volatile. The maximum POPA of the LT cycle is 3.04 kW/m^2. Figure 11b is the POPA characteristic analysis of the system. Before 1000 r/min, with the increase in rate, the system's POPA gradually decreased. At 1000–1900 r/min, with the increase of rate, the system's POPA first decreased and then increased. Beginning around 1900 r/min, with the increase of rate, the system's POPA gradually decreases. The maximum POPA is 1.75 kW/m^2.

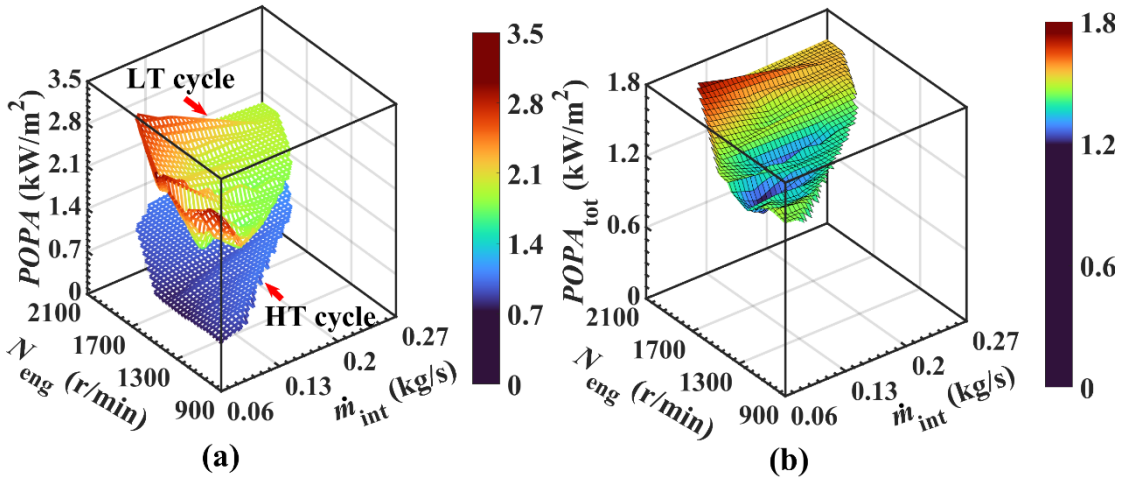

Figure 11. POPA of HT cycle, LT cycle and system under variable working conditions. (**a**) POPA characteristics analysis of different cycles. (**b**) POPA characteristic analysis of the system.

4.4.2. Key Variables

Figure 12 shows the POPA effect characteristics. Figure 12a shows the POPA effect characteristics of the condenser inlet temperature in different loops on the HT cycle. With the increase of the inlet temperature, the POPA of the HT cycle gradually decreases. Compared with inlet temperature, the change of the condenser inlet temperature in the LT cycle has less of an effect on the POPA of the HT cycle. Figure 12b shows the effect characteristics of POPA in the HT cycle. With the increase of pressure in the HT cycle, the POPA of the HT cycle gradually increased. As the inlet temperature of the HT cycle increases, the POPA of the HT cycle gradually decreases. The change of inlet temperature of the expander in the HT cycle has less effect on the POPA of the HT cycle.

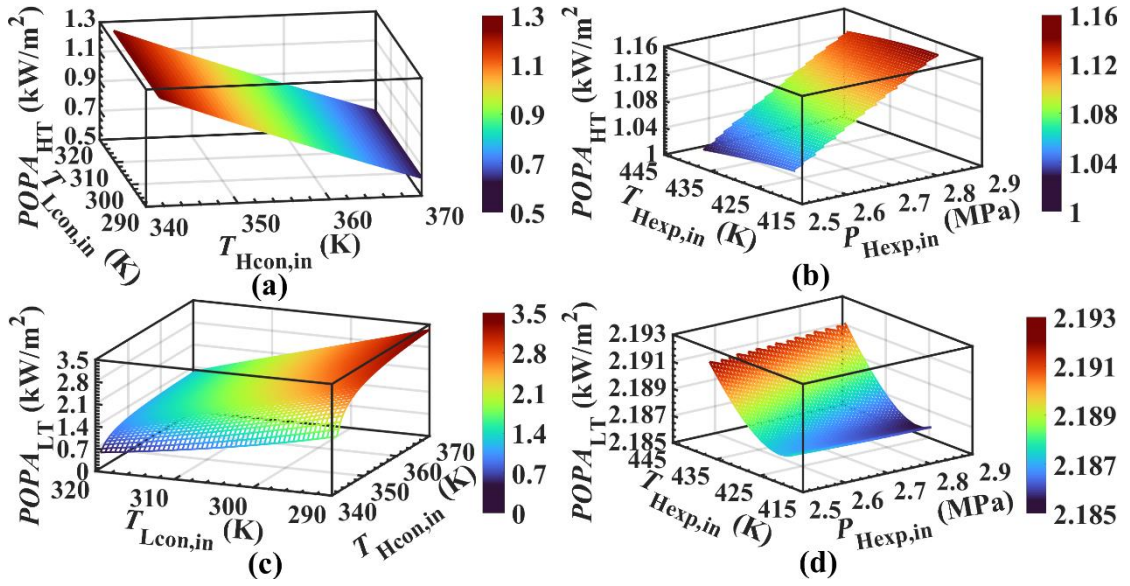

Figure 12. Influence characteristics of key variables on POPA of HT cycle and LT cycle. (**a**) POPA effect characteristics of the condenser inlet temperature in different loops on the HT cycle. (**b**) Effect characteristics of POPA in the HT cycle. (**c**) POPA effect characteristics on the LT cycle. (**d**) Effect characteristics on the HT cycle.

Figure 12c shows the POPA effect characteristics on the LT cycle. With the increase of inlet temperature of the HT cycle, the POPA of the LT cycle gradually increased. Figure 12d

shows the effect characteristics on the HT cycle. With the increase of inlet temperature of the expander of the HT cycle, the LT cycle of POPA gradually increased. Moreover, the growing trend of POPA becomes obvious.

Figure 13 shows the effect characteristics of total POPA. With the increase of inlet temperature of condenser in HT cycle, total POPA first increased and then decreased. Compared with the HT cycle, the condenser inlet temperature in the LT cycle has a better impact on total POPA. As the inlet pressure of the expander increases the HT cycle, POPA gradually increases. Compared with inlet temperature, the inlet pressure of the expander of the HT cycle has a better effect on POPA.

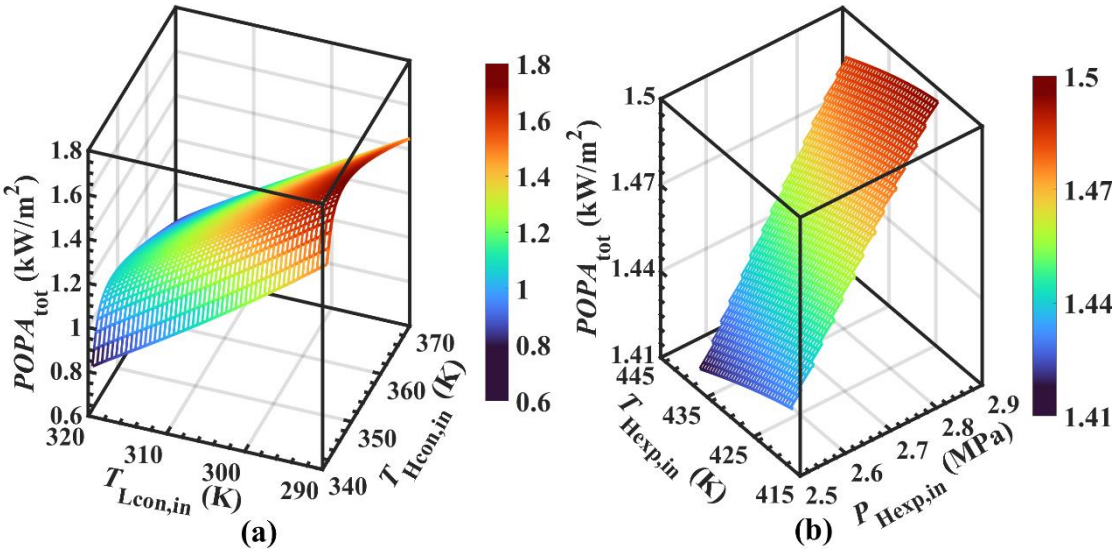

Figure 13. Influence characteristics of key variables on POPA. (**a**) Effect characteristics of total POPA in condenser parameter. (**b**) Effect characteristics of total POPA in expander parameter.

4.5. Exergy Destruction

4.5.1. Variable Working Conditions

Figure 14 shows the analysis of exergy destruction characteristics under variable working environments. Figure 14a shows the analysis of exergy destruction characteristics of different cycles. With the increase of speed, the exergy destruction of LT cycle gradually increases. The exergy destruction of the maximum of the LT cycle is 16.97 kW. The maximum exergy destruction of the HT cycle is 86.27 kW. Compared with speed, the intake flow has a better impact on exergy destruction of different cycles. Figure 14b shows the analysis of system exergy destruction characteristics. As the intake flow increases, system exergy destruction increases gradually. The maximum system exergy destruction is 103.24 kW.

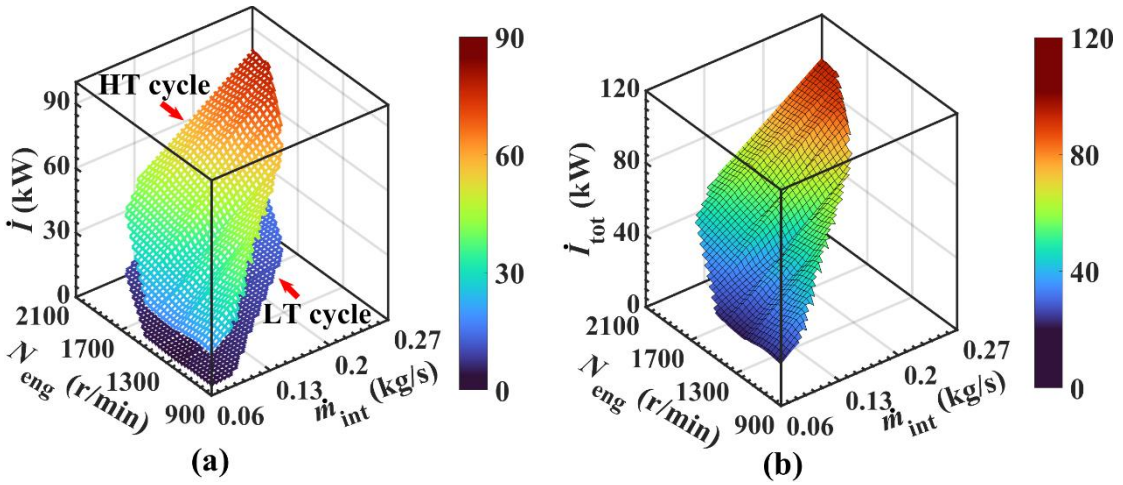

Figure 14. Exergy destruction of HT cycle, LT cycle and the system under variable working conditions. (**a**) Exergy destruction characteristics of different cycles. (**b**) System exergy destruction characteristics.

4.5.2. Key Variables

Figure 15 shows the influence of exergy destruction. Figure 15a shows the effect of exergy destruction in the HT cycle. As the inlet temperature of the condenser increases in the LT cycle, the exergy destruction of the HT cycle increases gradually. The change of the condenser inlet temperature in the HT cycle has less effect on the exergy destruction of the HT cycle. Figure 15b shows the effect of exergy destruction in the HT cycle. As inlet pressure of the expander increases in the HT cycle, the exergy destruction in the HT cycle gradually decreases. The change of expander inlet pressure of the HT cycle has little influence on the HT cycle exergy destruction.

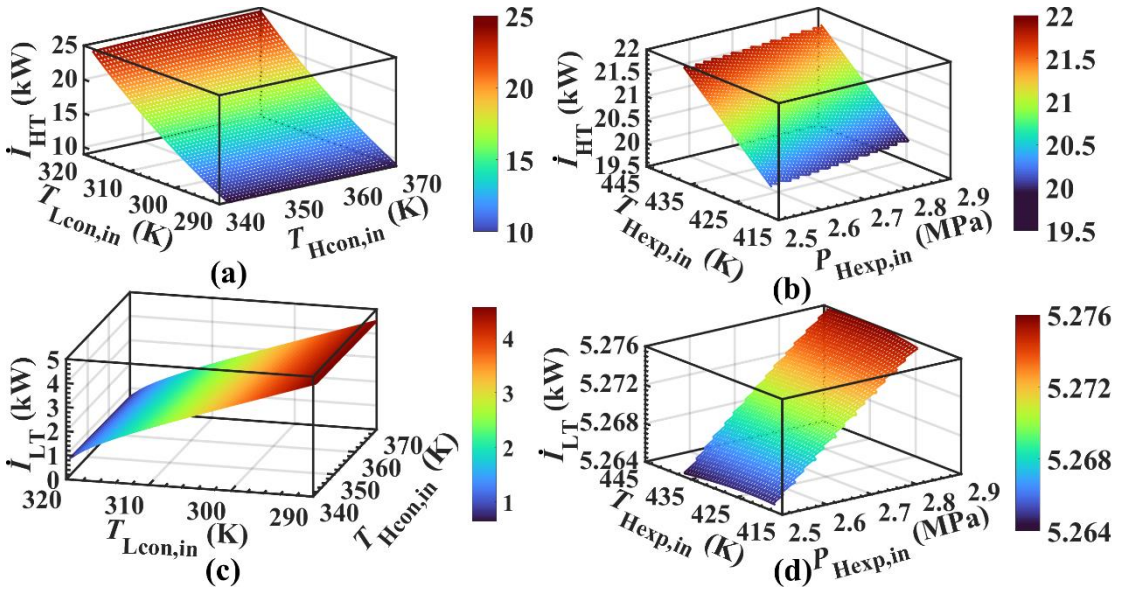

Figure 15. Influence characteristics of key variables on exergy destruction of HT cycle and LT cycle. (**a**) Effect of exergy destruction in the HT cycle. (**b**) Effect of exergy destruction in the HT cycle. (**c**) Effect of exergy destruction in the LT cycle. (**d**) Effect characteristics of exergy destruction in the HT cycle.

Figure 15c shows the effect of exergy destruction in the LT cycle. With the increase of the HT cycle condenser inlet temperature, the exergy destruction of the LT cycle gradually decreased. Compared with the condenser inlet temperature in the LT cycle, the change of

the condenser inlet temperature in the HT cycle has less influence on the exergy destruction of the LT cycle. Figure 15d shows the effect characteristics of exergy destruction in the HT cycle. With the increase of the expander inlet pressure in the HT cycle, the exergy destruction of LT cycle gradually increased. The exergy destruction of the LT cycle changes little as the inlet temperature of the expander of the HT cycle increases.

Figure 16 shows the effect characteristics of system exergy destruction. Figure 16a shows the effect characteristics of condenser inlet temperature in different cycles on exergy destruction. As the condenser inlet temperature increases in the HT cycle, the system exergy destruction increases gradually. Compared with the condenser inlet temperature in the HT cycle, the condenser inlet temperature in the LT cycle has a better effect on system exergy destruction. Figure 16b shows the effect characteristics of inlet temperature and pressure of the expander of the HT cycle for system exergy destruction. As the expander inlet pressure increases in the HT cycle, the system exergy destruction gradually decreases.

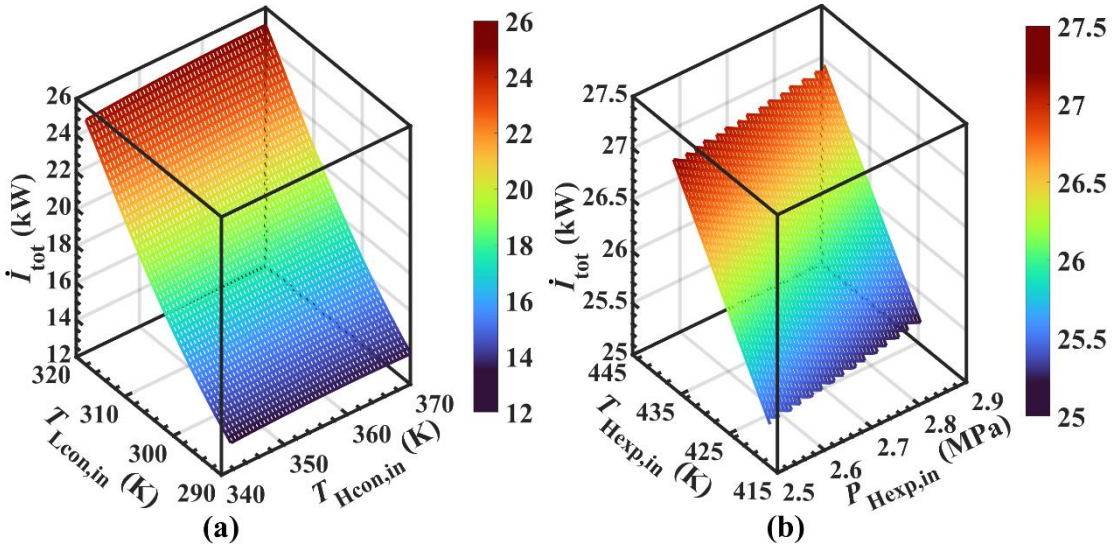

Figure 16. Influence characteristics of key variables on exergy destruction. (**a**) Effect characteristics of condenser inlet temperature in different cycles on exergy destruction. (**b**) Effect characteristics of inlet temperature and pressure of the expander of the HT cycle for system exergy destruction.

4.6. ECE

4.6.1. Variable Working Conditions

Figure 17 shows the effect analysis of direct ECE, indirect ECE and system ECE. Figure 17a shows the characteristic analysis of direct ECE and indirect ECE. As the intake flow increases, the direct ECE gradually increases. As speed increases, direct ECE gradually increases. Maximum direct ECE is 41.79 ton CO_2,eq. As the intake flow increases, the indirect ECE gradually increases. The maximum indirect ECE is 9.26 ton CO_2,eq. Compared with speed, the intake mass flow rate has a better effect on direct ECE and indirect ECE. Figure 17b shows the effect analysis in system ECE. As the intake rate increases, the total ECE gradually increases. With the increase of speed, the total ECE gradually increases. Maximum system ECE is 51.05 ton CO_2,eq.

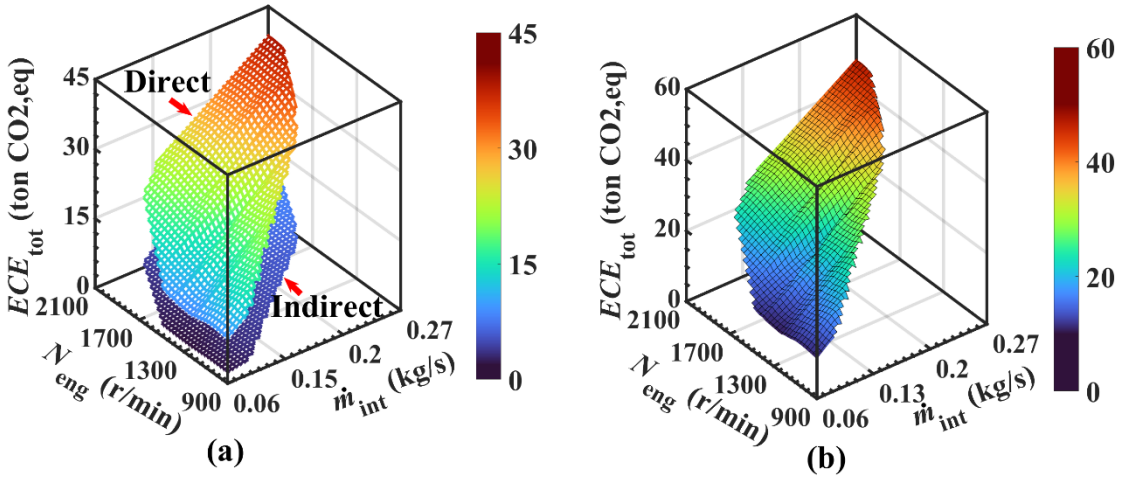

Figure 17. ECE of HT cycle, LT cycle and system under variable working conditions. (**a**) Direct ECE and indirect ECE. (**b**) System ECE.

4.6.2. Key Variables

Figure 18 shows the effect characteristics of direct ECE and indirect ECE. Figure 18a shows the effect characteristics of the inlet temperature of the condenser in different loops on direct ECE. With the increase of inlet temperature of the condenser in the LT cycle, the direct ECE of the HT cycle gradually decreased. Compared with the condenser inlet temperature in the LT cycle, the change of condenser inlet temperature in the HT cycle has less influence on the direct ECE of the HT cycle. Figure 18b shows the effect characteristics of the expander on the HT cycle. As pressure increases, the direct ECE of the HT cycle gradually increases.

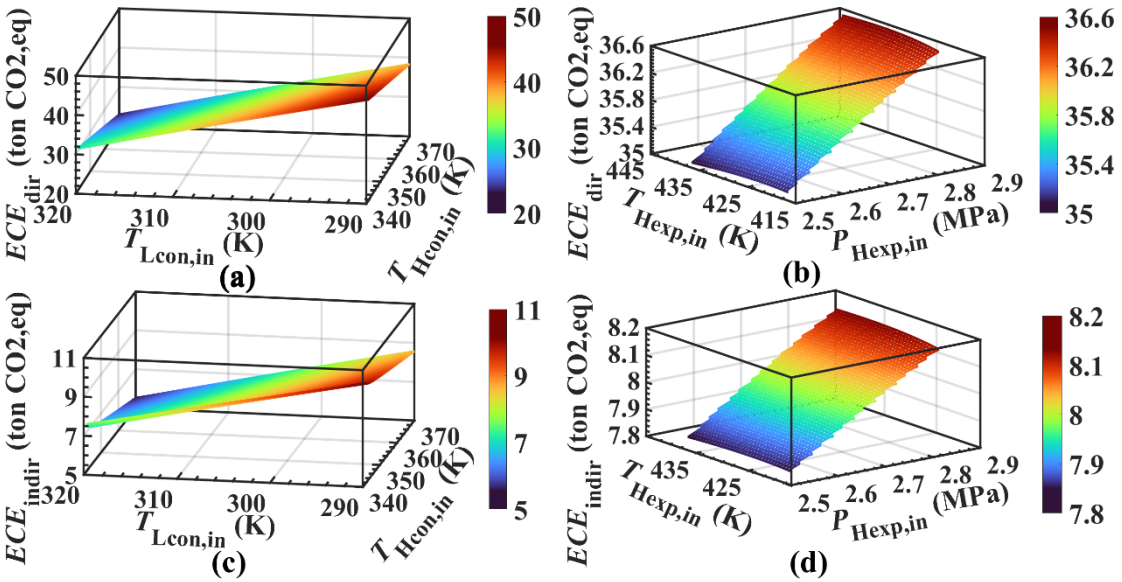

Figure 18. Influence characteristics of key variables on direct ECE and indirect ECE. (**a**) Effect characteristics of the inlet temperature of the condenser in different loops on direct ECE. (**b**) Effect characteristics of the expander on the HT cycle direct ECE. (**c**) Effect characteristics of the inlet temperature of the condenser in different loops on indirect ECE. (**d**) Effect characteristics of the expander on the HT cycle indirect ECE.

Figure 19 shows the effect characteristics of total ECE. Figure 19a presents the impact characteristics of condenser inlet temperature on system ECE. As condenser inlet temperature increases in the HT cycle, system ECE gradually decreases. With the increasing of

condenser inlet temperature in the LT cycle, system ECE decreases gradually. Compared with the condenser inlet temperature in the HT cycle, condenser inlet temperature in the LT cycle has more of an effect on system ECE. Figure 19b presents the impact of expander inlet temperature and pressure on the HT cycle on system ECE. With the increasing of inlet pressure in the HT cycle, system ECE gradually increases. With the increasing of inlet temperature in the HT cycle, the system ECE changes slightly. Compared with inlet temperature, the expander inlet pressure cycle exerts a greater impact on ECE.

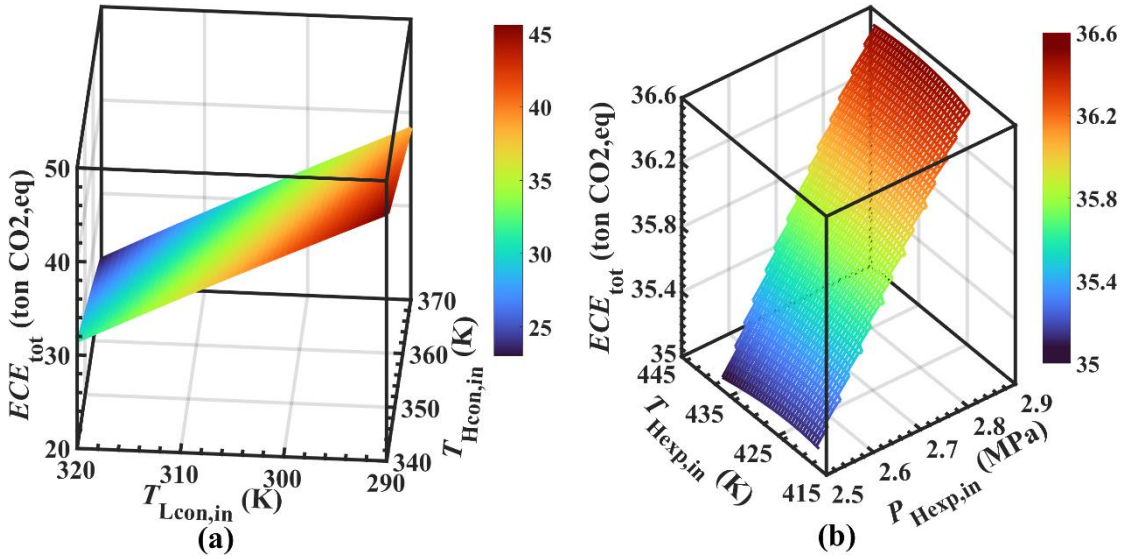

Figure 19. Influence characteristics of key variables on ECE. (**a**) Impact characteristics of condenser inlet temperature on system ECE. (**b**) Impact of expander inlet temperature and pressure on the HT cycle on system ECE.

4.7. Multi Objective Optimization and TOPSIS Selection

TOPSIS can make decisions on data difference through given data. TOPSIS processes the attributes in a definite direction to filter out the optimal values. Sample to optimal and sample to worst distance is then calculated by the distance scale. The assessment is based on closeness, and the value can be expressed as:

$$D_{i+} = \sqrt{\sum_{j=1}^{n}\left(F_{ij} - F_j^{ideal}\right)^2};\ D_{i-} = \sqrt{\sum_{j=1}^{n}\left(F_{ij} - F_j^{non\text{-}ideal}\right)^2} \tag{68}$$

Furthermore, the closeness can be expressed as follows:

$$C_i = \frac{D_{i-}}{D_{i+} + D_{i-}} \tag{69}$$

Figure 20 shows the DORC system thermodynamic multiobjective optimization and TOPSIS selection. The figure indicates that thermal efficiency and output power have a positive correlation. Apparently, to achieve higher thermal efficiency leads to higher output power. To achieve higher thermal efficiency and higher output power, however, which also leads to higher total exergy destruction. The optimal result of the parameters above for thermal efficiency, output power, and total exergy destruction are 14.27%, 37.11 kW, and 104.58 kW, respectively.

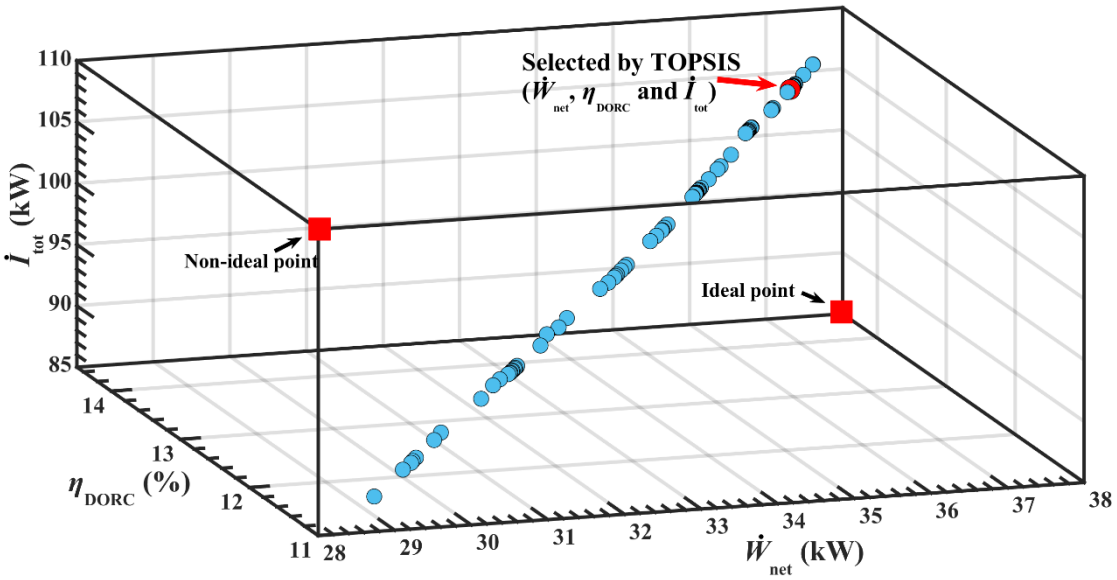

Figure 20. Multi objective optimization and TOPSIS selection.

5. Conclusions

The operation characteristics of CHG engines are fully considered, and the characteristics of different heat sources under variable environments are systematically analyzed. According to the structural characteristics, the thermodynamic, heat transfer and environmental model of DORC is built. Based on variation characteristics of multi-source heat energy of CNG engines, the recovery potential of DORC under full working conditions is systematically evaluated. According to the operating characteristics of different loops, the variation laws of loop performance under the influence of multiple parameters are analyzed. The laws of synergistic effects of multiple variables on system performance are analyzed by thermodynamic performance, heat transfer performance, thermoeconomic performance and environmental impact. The main conclusions are summarized as follows:

(1) Fluctuation of CNG engine environments makes characteristics of different heat sources significantly different. Compared with speed, intake flow has a better impact on the heat characteristics of intercooler and the exhaust heat transfer rate. The increase of intake flow will make the nonlinear relationship between speed and waste heat source of the intercooler gradually obvious. At the same time, the correlation between speed and the ration of the exhaust heat transfer rate will be significantly improved.

(2) The coupling relationship between engine and DORC is obviously affected by working conditions. Compared with speed, intake mass flow rate has a significant influence on power, POPA and exergy destruction of a loop. At the same time, the comprehensive performance of a system is obviously affected by intake flow. Under the disturbance of intake flow, the maximum power, heat transfer area and POPA of DORC are 36.42 kW, 23.34 m^2 and 1.75 kW/m^2, respectively.

(3) The coupling relationship between operating parameters makes the loop performance show a non-linear change. The increase of inlet temperature of the condenser of the HT cycle increases its correlation with heat transfer surface. The POPA change trend of the LT cycle gradually slowed down. The increase of inlet temperature of the condenser of the LT cycle reduces the correlation with the heat transfer surface.

(4) Under the synergistic influence of operating parameters in a loop, the correlation between variable and DORC performance is significantly different. Compared with the condenser inlet temperature in an HT cycle, the inlet temperature of the condenser of the LT cycle had a better effect on system power, POPA, ECE and exergy destruction. Compared with inlet temperature of the expander of the HT cycle, the inlet pressure of the expander of the HT cycle has a greater effect on system comprehensive performance.

The reliability and adaptability of working fluids are key to the comprehensive performance analysis and optimization of DORC. The working fluid thermophysical properties exert an important influence on operation performance, and the system performance presents significant differences with various working fluids. In future research, the impact of working fluid on the DORC system's working performance will be investigated.

Author Contributions: X.P.: Investigation, Conceptualization, Methodology, Software, Validation, Writing—Origi-nal Draft. B.Y.: Conceptualization, Methodology, Writing—Review & Editing, Supervision. H.Z. (Hongguang Zhang): Conceptualization, Methodology, Writing—Review & Editing. H.Z. (Hongzhi Zhang): Methodology, Writing—Review & Editing. J.L.: Writing—Review & Edit-ing. M.Y.: Writing—Review. K.N.: Review. Y.W.: Editing. All authors have read and agreed to the published version of the manuscript.

Funding: This work was sponsored by the Beijing Natural Science Foundation (Grant No. 3222024), and supported by State Key Laboratory of Engines, Tianjin University (Grant No. K2020-08). The authors would like to thank the reviewers for their valuable comments on this research.

Conflicts of Interest: The authors declare no conflict of interest.

Nomenclature

A	heat transfer area (m^2)
Bo	boiling number
b	channel spacing (m)
C_p	specific heat at constant pressure
c_t	temperature difference correction factor
d	diameter (m)
F	forced convective heat transfer enhancement factor
f	Darcy resistance coefficient
G	mass velocity ($kg/m^2 \cdot s$)
H	fuel low calorific value
h	specific enthalpy (kJ/kg)
I	exergy destruction (kW)
i	annual interest rate
K	overall heat transfer coefficient ($W/m^2 \cdot K$)
l	length (m)
M	molecular weight (kg/kmol)
$\dot{m}$	mass flow rate (kg/s)
Nu	Nusselt number
P	pressure (MPa)
p_r	reduced pressure
Pr	Prandtl number
$\dot{Q}$	heat transfer rate (kW)
q	heat flux ($kW/(m^2 \cdot K)$)
r_{fg}	enthalpy of vaporization (J/kg)
Re	Reynolds number
S	suppression factor
s	specific entropy
A	temperature (K)
$\dot{W}$	power output (kW)
w	channel width (m)

x	mass fraction
Greek letters	
λ	thermal conductivity (W/m·K)
β	rib effect coefficient
r	fouling resistance (m^2·K/W)
ε	correction factor
δ	fin height (m)
α	heat transfer coefficient (W/m^2·K)
μ	dynamic viscosity (N·s/m^2)
Subscripts	
cool	coolant
env	environment
eng	engine
exh	exhaust
eva	evaporator
exp	expander
eq	equivalent
f	fin
ft	fin-and-tube heat exchanger
fb	film boiling
h	hydraulic
in	inner
inter	intercooler
l	liquid
LT	lifetime or low temperature
nb	nucleate boiling
th	thermal
tp	two-phase
tot	total
out	outer
P	pressure (MPa) or pump
pl	plate heat exchanger
pre	preheater
tot	total
v	vapor
w	wall
wf	working fluid
6a-l	state points in HT loop
Acronyms	
CNG	compressed natural gas
DORC	dual loop organic Rankine cycle
ECE	emissions of CO_2 equivalent
HT	high temperature
IC	internal combustion
LT	low temperature
LMTD	logarithmic mean temperature difference
ORC	organic Rankine cycle
POPA	net power output per unit heat transfer area

References

1. Wang, E.H.; Zhang, M.R.; Meng, F.X.; Zhang, H.G. Zeotropic working fluid selection for an organic Rankine cycle bottoming with a marine engine. *Energy* **2022**, *243*, 123097. [CrossRef]
2. Zhao, Y.; Gao, C.H.; Li, C.J.; Sun, J.; Wang, C.Y.; Liu, Q.; Zhao, J. Energy and Exergy Analyses of Geothermal Organic Rankine Cycles Considering the Effect of Brine Reinjection Temperature. *Energies* **2022**, *15*, 6230. [CrossRef]
3. Lu, Y.J.; Roskilly, A.P.; Yu, X.L.; Jiang, L.; Chen, L.F. Technical feasibility study of scroll-type rotary gasoline engine: A compact and efficient small-scale Humphrey cycle engine. *Appl. Energy* **2018**, *221*, 67–74. [CrossRef]
4. Prasad, R.K.; Mustafi, N.; Agarwal, A.K. Effect of spark timing on laser ignition and spark ignition modes in a hydrogen enriched compressed natural gas fuelled engine. *Fuel* **2020**, *276*, 118071. [CrossRef]

5. Ping, X.; Yang, F.B.; Zhang, H.G.; Zhang, W.J.; Song, G.G.; Yang, Y.X. Prediction and optimization of isentropic efficiency of vortex pump under full operating conditions in Organic Rankine Cycle waste heat recovery system based on deep learning and intelligent algorithm. *Sustain. Energy Technol. Assess.* **2020**, *42*, 100898. [CrossRef]
6. Meng, F.X.; Wang, E.H.; Zhang, B. Possibility of optimal efficiency prediction of an organic Rankine cycle based on molecular property method for high-temperature exhaust gases. *Energy* **2021**, *222*, 119974.
7. Ping, X.; Yang, F.B.; Zhang, H.G.; Zhang, J.; Zhang, W.J.; Song, G.G. Introducing machine learning and hybrid algorithm for prediction and optimization of multistage centrifugal pump in an ORC system. *Energy* **2021**, *222*, 120007. [CrossRef]
8. Feng, Y.Q.; Xu, J.W.; He, Z.X.; Hung, T.C.; Shao, M.; Zhang, F.Y. Numerical simulation and optimal design of scroll expander applied in a small-scale organic rankine cycle. *Energy* **2022**, *260*, 124981. [CrossRef]
9. Xie, H.; Yang, C. Dynamic behavior of Rankine cycle system for waste heat recovery of heavy duty diesel engines under driving cycle. *Appl. Energy* **2013**, *112*, 130–141. [CrossRef]
10. Ping, X.; Yang, F.B.; Zhang, H.G.; Xing, C.D.; Wang, C.Y.; Zhang, W.J.; Wang, Y. Energy, economic and environmental dynamic response characteristics of organic Rankine cycle (ORC) system under different driving cycles. *Energy* **2022**, *246*, 123438. [CrossRef]
11. Ramli, W.R.B.W.; Pesyridis, A.; Gohil, D.; Alshammari, F. Organic Rankine Cycle Waste Heat Recovery for Passenger Hybrid Electric Vehicles. *Energies* **2020**, *13*, 4532. [CrossRef]
12. Wang, Z.Q.; Hu, Y.H.; Xia, X.X.; Zuo, Q.S.; Zhao, B.; Li, Z.X. Thermo-economic selection criteria of working fluid used in dual-loop ORC for engine waste heat recovery by multi-objective optimization. *Energy* **2020**, *197*, 117053. [CrossRef]
13. Zhi, L.H.; Hu, P.; Chen, L.X.; Zhao, G. Performance analysis and optimization of engine waste heat recovery with an improved transcritical-subcritical parallel organic Rankine cycle based on zeotropic mixtures. *Appl. Therm. Eng.* **2020**, *181*, 115991. [CrossRef]
14. Zhi, L.H.; Hu, P.; Chen, L.X.; Zhao, G. Thermodynamic analysis of an innovative transcritical CO2 parallel Rankine cycle driven by engine waste heat and liquefied natural gas cold. *Energy Convers. Manag.* **2020**, *209*, 112583. [CrossRef]
15. Song, J.; Li, X.Y.; Wang, K.; Markides, C.N. Parametric optimisation of a combined supercritical CO2 (S-CO2) cycle and organic Rankine cycle (ORC) system for internal combustion engine (ICE) waste-heat recovery. *Energy Convers. Manag.* **2020**, *218*, 112999. [CrossRef]
16. De Oliveira Neto, R.; Sotomonte, C.A.R.; Coronado, C.J.R.; Nascimento, M.A.R. Technical and economic analyses of waste heat energy recovery from internal combustion engines by the Organic Rankine Cycle. *Energy Convers. Manag.* **2016**, *129*, 168–179. [CrossRef]
17. Wang, X.; Shu, G.Q.; Tian, H.; Liu, P.; Jing, D.Z.; Li, X.Y. Dynamic analysis of the dual-loop Organic Rankine Cycle for waste heat recovery of a natural gas engine. *Energy Convers. Manag.* **2017**, *148*, 724–736. [CrossRef]
18. Ping, X.; Yao, B.F.; Zhang, H.G.; Yang, F.B. Thermodynamic, economic, and environmental analysis and multi-objective optimization of a dual loop organic Rankine cycle for CNG engine waste heat recovery. *Appl. Therm. Eng.* **2021**, *193*, 116980. [CrossRef]
19. Huang, H.Z.; Zhu, J.; Yan, B. Comparison of the performance of two different Dual-loop organic Rankine cycles (DORC) with nanofluid for engine waste heat recovery. *Energy Convers. Manag.* **2016**, *126*, 99–109. [CrossRef]
20. Ping, X.; Yao, B.F.; Zhang, H.G.; Yang, F.B. Thermodynamic analysis and high-dimensional evolutionary many-objective optimization of dual loop organic Rankine cycle (DORC) for CNG engine waste heat recovery. *Energy* **2021**, *236*, 121508. [CrossRef]
21. Ochoa, G.V.; Rojas, J.P.; Forero, J.D. Advance Exergo-Economic Analysis of a Waste Heat Recovery System Using ORC for a Bottoming Natural Gas Engine. *Energies* **2020**, *13*, 267. [CrossRef]
22. He, M.; Wang, E.H.; Zhang, Y.Y.; Zhang, W.; Zhang, F.J.; Zhao, C.L. Performance analysis of a multilayer thermoelectric generator for exhaust heat recovery of a heavy-duty diesel engine. *Appl. Energy* **2020**, *274*, 115298. [CrossRef]
23. Ping, X.; Yang, F.B.; Zhang, H.G.; Xing, C.D.; Zhang, W.J.; Wang, Y. Evaluation of hybrid forecasting methods for organic Rankine cycle: Unsupervised learning-based outlier removal and partial mutual information-based feature selection. *Appl. Energy* **2022**, *311*, 118682. [CrossRef]
24. Fouad, W.A. A combined heat, hydrogen and power tri-generation system based on the use of catalytic membrane reactors with a dual-loop organic Rankine cycle. *Energy Convers. Manag.* **2020**, *222*, 113255. [CrossRef]
25. Linnemann, M.; Priebe, K.P.; Heim, A.; Wolff, C.; Vrabec, J. Experimental investigation of a cascaded organic Rankine cycle plant for the utilization of waste heat at high and low temperature levels. *Energy Convers. Manag.* **2020**, *205*, 112381. [CrossRef]
26. Liu, X.Y.; Nguyen, M.Q.; He, M.G. Performance analysis and optimization of an electricity-cooling cogeneration system for waste heat recovery of marine engine. *Energy Convers. Manag.* **2020**, *214*, 112887. [CrossRef]
27. Surendran, A.; Seshadri, S. Performance investigation of two stage Organic Rankine Cycle (ORC) architectures using induction turbine layouts in dual source waste heat recovery. *Energy Convers. Manag.* **2020**, *6*, 100029. [CrossRef]
28. Mohammadkhani, F.; Yari, M. A 0D model for diesel engine simulation and employing a transcritical dual loop Organic Rankine Cycle (ORC) for waste heat recovery from its exhaust and coolant: Thermodynamic and economic analysis. *Appl. Therm. Eng.* **2019**, *150*, 329–347. [CrossRef]
29. Cavazzini, G.; Bari, S. Optimization of the Adsorption/Desorption Contribution from Metal-Organic-Heat-Carrier Nanoparticles in Waste Heat Recovery Applications: R245fa/MIL101 in Organic Rankine Cycles. *Energies* **2022**, *15*, 1138. [CrossRef]

30. Ping, X.; Yang, F.B.; Zhang, H.G.; Zhang, J.; Zhang, W.J. Elman and back propagation neural networks based working fluid side energy level analysis of shell-andtube evaporator in organic Rankine cycle (ORC) system. *Alex. Eng. J.* **2022**, *61*, 7339–7352. [CrossRef]
31. Feng, Y.Q.; Hung, T.C.; Zhang, Y.N.; Li, B.X.; Yang, J.F.; Shi, Y. Performance comparison of low-grade ORCs (organic Rankine cycles) using R245fa, pentane and their mixtures based on the thermoeconomic multi-objective optimization and decision makings. *Energy* **2015**, *93*, 2018–2029. [CrossRef]
32. Shu, G.Q.; Liu, P.; Tian, H.; Wang, X.; Jing, D.Z. Operational profile based thermal-economic analysis on an Organic Rankine cycle using for harvesting marine engine's exhaust waste heat. *Energy Convers. Manag.* **2017**, *146*, 107–123. [CrossRef]
33. Ping, X.; Yao, B.F.; Niu, K.; Yuan, M. A machine learning framework with intelligent algorithm for predicting the isentropic efficiency of hydraulic diaphragm metering pump in organic Rankine cycle system. *Front. Energy Res.* **2022**, *10*, 851513. [CrossRef]
34. Xu, B.; Li, X.Y. A Q-learning based transient power optimization method for organic Rankine cycle waste heat recovery system in heavy duty diesel engine applications. *Appl. Energy* **2021**, *286*, 116532. [CrossRef]
35. Douvartzides, S.L.; Tsiolikas, A.; Charisiou, N.D.; Souliotis, M.; Karayannis, V.; Taousanidis, N. Energy and Exergy-Based Screening of Various Refrigerants, Hydrocarbons and Siloxanes for the Optimization of Biomass Boiler–Organic Rankine Cycle (BB–ORC) Heat and Power Cogeneration Plants. *Energies* **2022**, *15*, 5513. [CrossRef]
36. Li, X.Y.; Xu, B.; Tian, H.; Shu, G.Q. Towards a novel holistic design of organic Rankine cycle (ORC) systems operating under heat source fluctuations and intermittency. *Renew. Sustain. Energy Rev.* **2021**, *147*, 111207. [CrossRef]
37. Ping, X.; Yang, F.B.; Zhang, H.G.; Xing, C.D.; Zhang, W.J.; Wang, Y.; Yao, B.F. Dynamic response assessment and multi-objective optimization of organic Rankine cycle (ORC) under vehicle driving cycle conditions. *Energy* **2023**, *263*, 125551. [CrossRef]
38. Li, X.Y.; Song, J.; Yu, G.P.; Liang, Y.C.; Tian, H.; Shu, G.Q.; Markides, C.N. Organic Rankine cycle systems for engine waste-heat recovery: Heat exchanger design in space-constrained applications. *Energy Convers. Manag.* **2019**, *199*, 111968. [CrossRef]
39. Zinsalo, J.M.; Lamarche, L.; Raymond, J. Performance analysis and working fluid selection of an Organic Rankine Cycle Power Plant coupled to an Enhanced Geothermal System. *Energy* **2022**, *245*, 123259. [CrossRef]
40. Ping, X.; Yang, F.B.; Zhang, H.G.; Wang, Y.; Lei, B.; Wu, Y.T. Performance limits of the single screw expander in organic Rankine cycle with ensemble learning and hyperdimensional evolutionary many-objective optimization algorithm intervention. *Energy* **2022**, *245*, 123254. [CrossRef]
41. Zukauskas, A. Heat Transfer from Tubes in Crossflow. *Adv. Heat Transf.* **1972**, *8*, 93–160.
42. Gnielinski, V. New equations for heat mass transfer in turbulent pipe and channel flows. *Int. J. Chem. Eng.* **1976**, *16*, 359–368.
43. Liu, Z.; Winterton, R.H.S. A general correlation for saturated and subcooled flow boiling in tubes and annuli, based on a nucleate pool boiling equation. *Int. J. Heat Mass Transf.* **1991**, *34*, 2759–2766. [CrossRef]
44. Ghiaasiaan, S.M. *Two-Phase Flow, Boiling and Condensation in Conventional and Miniature Systems*; Cambridge University Press: Cambridge, UK, 2008; pp. 321–353.
45. Ping, X.; Yang, F.B.; Zhang, H.G.; Zhang, W.J.; Zhang, J.; Song, G.G.; Wang, C.Y.; Yao, B.F.; Wu, Y.T. Prediction and optimization of power output of single screw expander in organic Rankine cycle (ORC) for diesel engine waste heat recovery. *Appl. Therm. Eng.* **2021**, *182*, 116048. [CrossRef]
46. Sanaye, S.; Khakpaay, N. Thermo-economic multi-objective optimization of an innovative cascaded organic Rankine cycle heat recovery and power generation system integrated with gas engine and ice thermal energy storage. *J. Energy Storage* **2020**, *32*, 101697. [CrossRef]
47. Zhao, Y.J.; Wang, J.F. Exergoeconomic analysis and optimization of a flash-binary geothermal power system. *Appl. Energy* **2016**, *179*, 159–170. [CrossRef]
48. García-Cascales, J.R.; Vera-García, F.; Corberán-Salvador, J.M.; Gonzálvez-Maciá, J. Assessment of boiling and condensation heat transfer correlations in the modelling of plate heat exchangers. *Int. J. Refrig.* **2007**, *30*, 1029–1041. [CrossRef]
49. Tian, H.; Shu, G.Q.; Wei, H.Q.; Liang, X.Y.; Liu, L.N. Fluids and parameters optimization for the organic Rankine cycles (ORCs) used in exhaust heat recovery of Internal Combustion Engine (ICE). *Energy* **2012**, *47*, 125–136. [CrossRef]
50. Liu, Q.; Shen, A.J.; Duan, Y.Y. Parametric optimization and performance analyses of geothermal organic Rankine cycles using R600a/R601a mixtures as working fluids. *Appl. Energy* **2015**, *148*, 410–420. [CrossRef]
51. Wang, S.K.; Liu, C.; Ren, J.Z.; Liu, L.; Li, Q.B.; Huo, E.G. Carbon footprint analysis of organic rankine cycle system using zeotropic mixtures considering leak of fluid. *J. Clean. Prod.* **2019**, *239*, 118095. [CrossRef]
52. Fergani, Z.; Touil, D.; Morosuk, T. Multi-criteria exergy based optimization of an Organic Rankine Cycle for waste heat recovery in the cement industry. *Energy Convers. Manag.* **2016**, *112*, 81–90. [CrossRef]
53. Ping, X.; Yang, F.B.; Zhang, H.G.; Xing, C.D.; Yao, B.F.; Wang, Y. An outlier removal and feature dimensionality reduction framework with unsupervised learning and information theory intervention for organic Rankine cycle (ORC). *Energy* **2022**, *254*, 124268. [CrossRef]
54. Ping, X.; Yang, F.B.; Zhang, H.G.; Xing, C.D.; Yu, M.Z.; Wang, Y. Investigation and multi-objective optimization of vehicle engine-organic Rankine cycle (ORC) combined system in different driving conditions. *Energy* **2023**, *263*, 125672. [CrossRef]
55. Zhang, C.; Liu, C.; Xu, X.X.; Li, Q.B.; Wang, S.K. Energetic, exergetic, economic and environmental (4E) analysis and multi-factor evaluation method of low GWP fluids in trans-critical organic Rankine cycles. *Energy* **2019**, *168*, 332–345. [CrossRef]
56. Yang, F.B.; Cho, H.J.; Zhang, H.G.; Zhang, J. Thermodynamic multi-objective optimization of a dual loop organic Rankine cycle (ORC) for CNG engine waste heat recovery. *Appl. Energy* **2017**, *205*, 1100–1118. [CrossRef]

57. Yaglı, H.; Koç, Y.; Kalay, H. Optimisation and exergy analysis of an organic Rankine cycle (ORC) used as a bottoming cycle in a cogeneration system producing steam and power. *Sustain. Energy Technol. Assess.* **2021**, *44*, 100985.
58. Köse, Ö.; Koç, Y.; Yaglı, H. Energy, exergy, economy and environmental (4E) analysis and optimization of single, dual and triple configurations of the power systems: Rankine Cycle/Kalina Cycle, driven by a gas turbine. *Energy Convers. Manag.* **2021**, *227*, 113604. [CrossRef]
59. Koç, Y.; Yağlı, H.; Kalay, I. Energy, Exergy, and Parametric Analysis of Simple and Recuperative Organic Rankine Cycles Using a Gas Turbine–Based Combined Cycle. *J. Energy Eng.* **2020**, *146*, 04020041. [CrossRef]